Aus der Abteilung für Klinische Pharmakologie

Medizinische Klinik und Poliklinik IV, Klinikum der Universität München

RIG-I-based immunotherapy of hepatocellular carcinoma: target validation and mechanisms of action *in vivo*

Dissertation

zum Erwerb des Doctor of Philosophy (Ph.D.)

an der Medizinischen Fakultät der

Ludwig-Maximilians-Universität München

vorgelegt von

Laura Posselt

aus

München

am

4. Dezember 2018

Supervisor: Prof. Dr. med. Max Schnurr

Co-supervision: PD Dr. rer. biol. hum. Peter Düwell

                     Dr. rer. nat. Lars König

Second expert: Prof. Dr. Simon Rothenfußer

Dean: Prof. Dr. med. dent. Reinhard Hickel

Date of oral defense: July 25th, 2019

Table of contents

Summary

Hepatocellular carcinoma (HCC) is the most common type of primary liver cancer. It is characterized by aggressive growth and poor prognosis. Despite progress in the medical management, treatment options are still limited and median survival for patients with advanced tumors is less than one year. New therapeutic interventions are therefore urgently needed.

The cytosolic helicase retinoic acid-inducible gene I (RIG-I) is an immune receptor for viral 5'-triphosphate-RNA (ppp-RNA) and its activation triggers innate and adaptive immunity via induction of type I interferon (IFN) and proinflammatory cytokines. In addition, it promotes an immunogenic form of cell death in tumor cells.

This project focused on the development of a ppp-RNA targeting RIG-I for HCC therapy. The aims of the study were to evaluate RIG-I as a potential therapeutic target in murine and human HCC cell lines and to assess the efficacy and mode of action of a RIG-I-based immunotherapy in an orthotopic HCC mouse model. This work revealed that RIG-I is expressed in human HCC tissue as well as in murine (RIL-175, Hep-55.1C, Hepa1-6) and human HCC cell lines (Huh7, Hep3B). It could be demonstrated that ppp-RNA treatment leads to the induction of IFN-β, MHC-I/HLA, IP-10 and cell death in all tested cell lines, indicating a functional RIG-I signaling pathway in HCC. After having established two orthotopic HCC mouse models (RIL-175- and Hep-55.1C-based), the efficacy and mode of action of ppp-RNA immunotherapy was investigated *in vivo*. It was demonstrated that mice bearing RIL-175 tumors strongly benefited from a systemic ppp-RNA therapy, whereas the immunotherapy did not show any effect in the Hep-55.1C model. The fundamental difference between the two models regarding the treatment efficacy could not be clarified in this work. Analysis of immune cell activation showed that splenic $CD4^+$ and $CD8^+$ T and NK cells, as well as NK cells at the tumor site were activated upon systemic ppp-RNA administration. However, depletion of NK cells did not alter the treatment effect. In contrast, the therapy was completely dependent on functional $CD4^+$ and $CD8^+$ T cells. This observation was corroborated by the fact that surviving mice surmounted a robust memory response upon rechallenge with the same tumor cells. Mice deficient for either MAVS or IFNAR1 still responded to therapy pointing towards an intra-tumoral rather than a host-specific RIG-I signaling response. The combination of RIG-I-based immunotherapy and PD-1 checkpoint inhibition resulted in a synergistic therapeutic effect in the RIL-175 mouse model, serving as a promising approach for a therapy in the clinical setting. In sum, this project provides evidence that ppp-RNA immunotherapy bears potential for the treatment of HCC deserving further evaluation.

1 Introduction

1.1 Clinical occurrence of hepatocellular carcinoma

Hepatocellular carcinoma (HCC) is a primary and malignant tumor of the liver tissue and one of the most incident cancer types worldwide, with men being three times more affected than women. Causes for disease development are frequently based on chronic inflammatory reactions of the liver tissue. Liver cirrhosis, an irreversible scarring of the liver tissue, as consequence of chronic infections, is often the root cause for HCC development (Bertuccio *et al.*, 2017; Sanyal *et al.*, 2010; Venook *et al.*, 2010).

Patients suffering from chronic liver cirrhosis and/or hepatitis B infection are at high risk for hepatocellular carcinoma. The increase in incidence of HCC of recent years is also associated with non-alcoholic fatty liver disease (NAFLD) in the consequence of obesity. Non-alcoholic steatohepatitis (NASH) belongs to the group of NAFLD and is an inflammatory disease of the liver tissue potentially leading to the induction and progression of liver fibrosis and cirrhosis, respectively. Also hepatitis C-associated or alcohol consumption-induced liver cirrhosis poses an increased risk to consequently coming down with HCC (reviewed in Leitlinienprogramm Onkologie, 2013).

1.2 Immune landscape of hepatocellular carcinoma

The immune system plays a crucial role in the development of HCC. Some immunological aspects that positively favor tumor growth are summarized below.

1.2.1 The immunosuppressive mircoenvironment of the liver

The liver is the body's largest excretory organ. During its crucial role in the detoxification process of the body it is exposed to a massive number of antigens contained in the blood and toxins derived from metabolic processes and the intestine. The liver has therefore established an intrinsic tolerability in order to avoid damage from autoimmunity in the presence of harmless antigens. The tolerogeneity of naïve T cells is mediated by liver sinusoidal endothelial cells (LSEC), Kupffer cells and dendritic cells (DC) via antigen-presentation. Further immunosuppressive mechanisms in order to inhibit T cell and NK cell activity include for example: the secretion of IL-10 by Kupffer cells and of TGF-β by Kupffer cells and LSEC, the downregulation of the co-stimulatory molecule CD80 on the LSEC as well as the expression of the immune checkpoint inhibitor Programmed cell death 1 ligand 1 (PD-L1) on hepatocytes, hepatic stellate cells and LSEC (Figure 1). All these factors mentioned, are supposed to also play an essential role in HCC development and for the tumor´s evasion from the host´s immune response (reviewed in Hato *et al.*, 2014; Makarova-Rusher *et al.*, 2015).
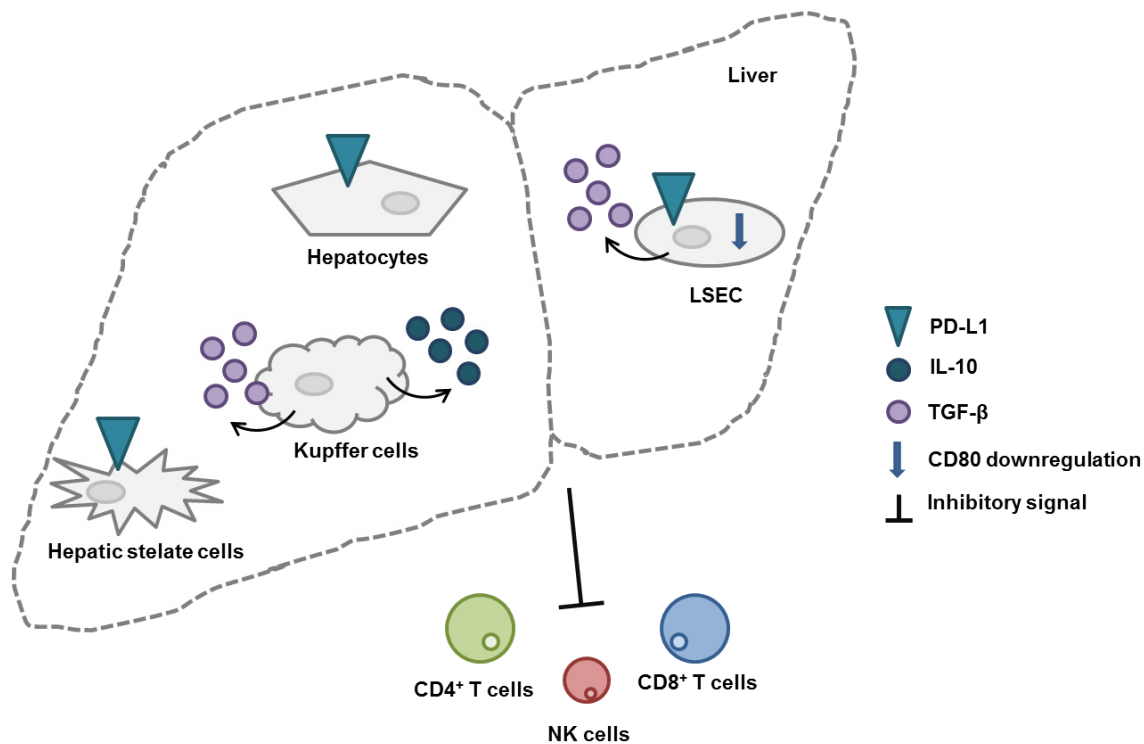
Figure 1: Scheme of the immunosuppressive microenvironment of the liver. Depicted in simplified terms are the immunosuppressive mechanisms mediated by liver cells in order to inhibit T cell and NK cell activity which include the secretion of IL-10 by Kupffer cells and of TGF-β by Kupffer cells and liver sinusoidal endothelial cells (LSEC), the downregulation of the co-stimulatory molecule CD80 on the LSEC as well as the expression of PD-L1 on hepatocytes, hepatic stellate cells and LSEC (modified from Makarova-Rusher *et al.*, 2015).

1.2.2 Immune checkpoint surveillance in oncogenesis

Chronic inflammation, such as HBV or HCV infection, is often the root cause for the development of primary liver cancer. Suppressive immune cells, for example regulatory T cells (T_{reg}), attracted by the inflamed tissue, and the continuous expression of anti-inflammatory cytokines, such as TGF-β, positively impact tumor escape mechanisms and tumorigenesis. Recent findings suggest, that proteins involved in the immune checkpoint surveillance play a key role in mediating tumor evasion and progression. Focusing on the immune checkpoint receptor PD-1, it was shown that its expression on intrahepatic lymphocytes positively correlates with the degree of chronic viral infection and has also been linked to the reduced effector function of T cells. Building on recent findings, the expression of immune checkpoint inhibitors is thought to mediate immune tolerance to tumor antigens thereby promoting tumor growth. Several findings show that intra-tumoral myeloid derived suppressor cells (MDSC) and T_{reg} inhibit the NK and T cell response via the PD-1/PD-L1 axis thereby helping tumor cells to evade the immune system. But also the immunosuppressive environment of the liver *per se* inhibits the lymphocyte-mediated tumor cell clearance through the expression of PD-L1 and the secretion of immunosuppressive cytokines by Kupffer cells,

hepatocytes, hepatic stellate cells and LSEC (reviewed in Hato *et al.*, 2014; Makarova-Rusher *et al.*, 2015).

1.3   Standard of care

HCC is characterized by aggressive growth and poor prognosis. It is most of the time diagnosed at an advanced stage, which significantly limits treatment options.

Treatment strategies are based on clinical stage of the tumor (Barcelona Clinic Liver Cancer Group classification) and performance status of the patient. Treatment is planned either in a curative intent or palliative if complete tumor control is unlikely to be achieved. Curative options include primary or secondary resection of tumor, liver transplantation or local ablation with either radiofrequency ablation (RFA) or percutaneous ethanol injection (PEI), leading to a five-year survival of 50-70 %. Palliative treatment includes transarterial chemoembolisation (TACE), radioembolisation or systemic treatment with the tyrosine kinase inhibitor sorafenib. Systemic chemotherapy has proven little to no benefit. The median survival rate is around 16 months. For patients with end stage liver disease the only option is best supportive care (BSC) with a survival rate less than three months (reviewed in Leitlinienprogramm Onkologie, 2013).

Several clinical trials have been conducted with the tyrosine kinase inhibitor sorafenib. Modest to effective and well tolerated results were observed depending on the severity of liver cirrhosis and metastatic spread (Abou-Alfa *et al.*, 2006; Cheng *et al.*, 2009; Llovet *et al.*, 2008; Pinter *et al.*, 2009; Yau *et al.*, 2009). As the first systemic therapy showing favor to the survival of patients suffering from advanced HCC, sorafenib was approved in 2005 by the Food and Drug Administration (FDA) and in 2007 by the European Medicines Agency (EMA) for the treatment of HCC (European Medicines Agency, 2011; Food and Drug Administration, 2013; Kane *et al.*, 2009), being now under suspicion to enhance metastasis formation (Zhang *et al.*, 2012). In addition, since the last years, numerous cases have been reported in which HCC patients show resistance to sorafenib. The reason for this is still under investigation (reviewed in Chen *et al.*, 2015).

1.4   Immunotherapy of hepatocellular carcinoma

Despite progress in the medical management, the incidence and the mortality rate of patients suffering from HCC are still increasing (Wong *et al.*, 2017). New therapeutic approaches are therefore urgently needed. Novel concepts of the clinical development of HCC therapy strongly focus on immunotherapeutic strategies. The main approaches are summarized in the following.

1.4.1 Current concepts of clinical development

1.4.1.1 Immunomodulators

1.4.1.1.1 Interferons

Interferons (IFN) are cytokines initially discovered by their anti-viral capacity. The anti-tumoral potential of IFN-α, -β and -γ was investigated for HCC therapy and was reported to be sufficient by inducing tumor cell death. In this regard, the question which type of IFN is more efficient is still under debate. However, much more cases using IFN-α have been reported (reviewed in Hong *et al.*, 2015). IFN-α treatment alone was considered not to be sufficient for HCC therapy, but was reported beneficial in an adjuvant setting in combination with 5-fluorouracil (Kasai *et al.*, 2012; Obi *et al.*, 2006; Sakon *et al.*, 2002). Adjuvant IFN-α therapy was further described to be save and to prolong recurrence free period post-surgery and after TACE treatment for unresectable HCC (Lee *et al.*, 2013; Li *et al.*, 2009).

1.4.1.1.2 Interleukins

Interleukins are cytokines that are involved in the regulation of inflammation. These characteristics have been utilized for cancer therapy in order to boost the anti-tumoral immune response. However, only few clinical studies with low numbers of patients with HCC have been conducted so far (reviewed in Hong *et al.*, 2015). Lygidakis *et al.* (1995) reported, that chemotherapy accompanied by high dose IFN-γ and IL-2 induced tumor necrosis and led to the reduction of AFP serum levels in patients with advanced HCC. The same was seen in a study reported by Sangro *et al.* (2004), where nine patients with primary liver cancer were treated with an IL-12 producing adenovirus. In the context of an IL-based anti-tumor therapy further investigations and the conduct of clinical trials with sufficient patient numbers are needed to confirm existing data (reviewed in Hong *et al.*, 2015).

1.4.1.2 Cancer vaccines

One further approach for the treatment of HCC is to take advantage of tumor-associated antigens (TAA) for the development of a cancer vaccine-based immunotherapy. Therefore, one challenge is the heterogeneity of HCC and thus pining down antigens which are characteristic and more or less specific for the tumor tissue. The most studied candidates reported for peptide-based vaccines are the TAA AFP, glypican 3 (GPC3) and telomerase reverse transcriptase (TERT), which are highly over-expressed in HCC (reviewed in Hong *et al.*, 2015). The first pilot study with this in mind was reported by Butterfield *et al.* (2003) investigating the efficacy of T cells specific for a HLA-A-restricted AFP peptide in HCC patients. The study revealed a strong immune response mediated by AFP-specific T cells, in the sense that T cells specific for AFP and also their expansion could be demonstrated *in vivo*. Further studies in this context are ongoing. The major challenges will be to overcome

the immunosuppressive microenvironment of HCC and to identify more specific TAA for the induction of a strong CD8$^+$ and also CD4$^+$ T cell response. Also combinatorial strategies are currently under discussion (reviewed in Buonaguro *et al.*, 2013).

1.4.1.3 Checkpoint inhibition

Huge progress has been made in melanoma immunotherapy during the last years, bringing also benefit for the treatment of several other solid tumor entities. Successful therapeutic approaches were made in regard to checkpoint inhibition with a special focus on the Programmed cell death protein 1 (PD-1)/Programmed cell death 1 ligand 1 (PD-L1) axis. Nivolumab and pembrolizumab are humanized monoclonal antibodies binding to the T cell receptor PD-1, which in turn interferes with the binding of PD-1 to its ligand PD-L1 in the tumor microenvironment, thereby blocking the tumor-mediated inhibition of T cell signaling. Binding of PD-1 to its ligand PD-L1, which is also expressed on antigen presenting cells, inhibits T cell receptor mediated IL-2 expression and T cell proliferation. This inhibition showed great success in prolonging survival and improving quality of life of patients with advanced melanoma. Both antibodies nivolumab and pembrolizumab have recently been approved by the EMA and the FDA for the treatment of melanoma (European Medicines Agency, 2017a, 2017b; Food and Drug Administration, 2017a, 2017b). Due to the great achievements made in melanoma research using checkpoint inhibitors, a logical consequence is trying to derive benefit for HCC treatment. Truong *et al.* (2016) reported first about a patient benefiting from pembrolizumab therapy after sorafenib treatment had failed. Several phase I/II and III studies are meanwhile ongoing using pembrolizumab and nivolumab, respectively, as single or concomitant therapy (ClinicalTrials.gov, 2018a, 2018b). El-Khoueiry *et al.* (2017) recently reported that the treatment with nivolumab led to a profound anti-tumor effect with an objective response rate of 15-20 % resulting in tumor reduction along with a positive impact on the overall survival of patients with advanced HCC.

1.4.1.4 Chimeric antigen receptors

One method used for immunotherapy of HCC is the adoptive transfer of immune cells. Cytokine-induced immune cells (CIK) produced and expanded from peripheral blood, tumor infiltrating lymphocytes (TIL) isolated from tumor tissue and engineered T cells genetically modified to express a tumor-specific chimeric antigen receptor (CAR) are examined (reviewed in Prieto *et al.*, 2015). The latter, also known as CAR T cells, have already been successfully used in hemato-oncological malignant diseases (Maus *et al.*, 2014). CAR T cells directed against the tumor-associated antigen (TAA) glypican 3 (GPC3) were already tested in mouse models of HCC opening up a promising therapeutic option *(Li et al., 2018)*. First results from clinical studies in the context of HCC therapy are yet to come.

1.4.1.5   Oncolytic viruses

A new approach in the field of immunotherapy is the use of oncolytic viruses (OV). These are viruses bearing a natural tropism for cancer cells and viruses whose capsid has been engineered carrying proteins that bind to tumor specific receptors, respectively. The infection of tumor cells with OV induces an immunogenic form of cell death: upon infection of tumor cells and subsequent cell lysis, antigen presenting cells (APC) recognize damage-associated molecular patterns (DAMP) derived from lysed tumor cells and pathogen-associated molecular patterns (PAMP) derived from the oncolytic viruses. As a consequence, CD8$^+$ T cell priming takes place in secondary lymphoid organs by the activated APC resulting in a tumor antigen-specific T cell response. In addition, CD8$^+$ T cells are recruited by the upregulation of MHC class I on the tumor cell surface due to the viral infection, which leads to a T cell receptor (TCR)-mediated killing of tumor cells (reviewed in Bommareddy *et al.*, 2018). In 2015 the first OV-based immunotherapy for the treatment of melanoma was approved by the FDA (Pol *et al.*, 2016). In the context of HCC therapy, Zhang *et al.* (2017) showed that the treatment with an OV sensitized towards HCC at low MOI results in an enhanced oncolytic capacity and effectively kills HCC cells *in vitro* and *in vivo*. In addition, the OV-based therapy revealed a tolerable safety profile in non-human primates. Abdullahi *et al.* (2018) recently reported on a novel chimeric OV for HCC therapy with an enhanced safety profile regarding off-target effects in liver and brain. Another approach was taken by Chen *et al.* (2017) who successfully combined OV therapy with adoptive T cell transfer to enhance the anti-tumoral capacity of the adopted T cells in an HCC mouse model.

1.4.2   RIG-I-like helicases for the therapy of hepatocellular carcinoma

One possible way to direct the immune system against the tumor is to mimic a viral infection of the tumor tissue itself. The immune system offers a plethora of germline-encoded receptors for the detection and elimination of invading pathogens such as bacteria and viruses called pathogen recognition receptors (PRR). The detection of certain viruses is carried out, amongst others, via so called retinoic acid-inducible gene I (RIG-I)-like helicases (RLH) with its well-described members RIG-I and melanoma differentiation-associated antigen 5 (MDA5) (reviewed in Takeuchi and Akira, 2008). The activation of RLH in tumor cells bears potential for anti-tumor immunotherapy. The actual concept is described below.

1.4.2.1   Biology and function of RIG-I-like helicases

RIG-I and MDA5 are ubiquitously expressed cytoplasmic receptors which induce antiviral immune responses by sensing viral nucleic acids. This results in an adaptive immune response and induces apoptosis of infected cells. The helicases are composed of: a N-terminal caspase-recruitment domain (CARD) responsible for signaling transduction, a conserved helicase domain and a C-terminal regulatory domain (CTD), which unfolds and

senses bound viral nucleic acid (Luo *et al.*, 2011). A special focus in this work is on the cytosolic helicase RIG-I, which is the ligand of double-stranded 5'-triphosphate- and double-stranded 5'-diphosphate-RNA (Goubau *et al.*, 2014; Hornung *et al.*, 2006). Activation of RIG-I leads to downstream signaling via the mitochondrial antiviral-signaling protein (MAVS) and activates the transcription factors IFN regulatory factor 3 and 7 (IRF3/7), Nuclear factor kappa-light-chain-enhancer of activated B-cells (NF-κB), and Mitogen-activated protein (MAP) kinase signaling (Schmidt *et al.*, 2009). This leads to the secretion of type I IFN and inflammatory cytokines, such as IP-10, triggering an adaptive immune cell response by the attraction and activation of dendritic cells (DC) and natural killer cells (NK cells). This again leads to the recruitment of cytotoxic T lymphocytes (CTL) via IFN-γ secretion (reviewed in Iwasaki and Medzhitov, 2010; Kaneda, 2013). For the sake of completeness, I want to also mention the third member of the RLH-family: laboratory of genetics and physiology 2 (LGP2). This protein differs in structure from the other two RLH, as it lacks a CARD domain. LGP2 is thought to act as a regulator of RIG-I and MDA5 during RLH signaling, but its exact function is not yet fully elucidated (reviewed in Ahmad and Hur, 2015).

1.4.2.2   RIG-I as target structure for therapy of hepatocellular carcinoma

The activation of RIG-I bears therapeutic potential, since its signaling pathway triggers an adaptive immune response and leads to the induction of apoptosis of infected cells, as already described in section 1.4.2.1. Mimicking a viral infection by synthetic or *in vitro*-transcribed RNA sensed by RLH, has been shown to induce the intrinsic mitochondrial apoptosis pathway leading to tumor cell death (Besch *et al.*, 2009). In addition, our research group could recently demonstrate that therapy of pancreatic tumors with RLH ligands induced a form of immunogenic tumor cell death with enhanced antigen presentation by DC and activation of tumor-directed T cells. Furthermore, it sensitized tumor cells towards CD95-mediated killing by immune cells *in vitro* (Duewell *et al.*, 2014). In addition the modification of siRNA as 5'-triphosphate-siRNA (5'-ppp-siRNA) allows combining gene silencing of oncogenic target genes with RIG-I activation via the 5'-ppp moiety (Duewell *et al.*, 2014; Ellermeier *et al.*, 2013; Petrocca and Lieberman, 2008; Poeck *et al.*, 2008) (Figure 2).
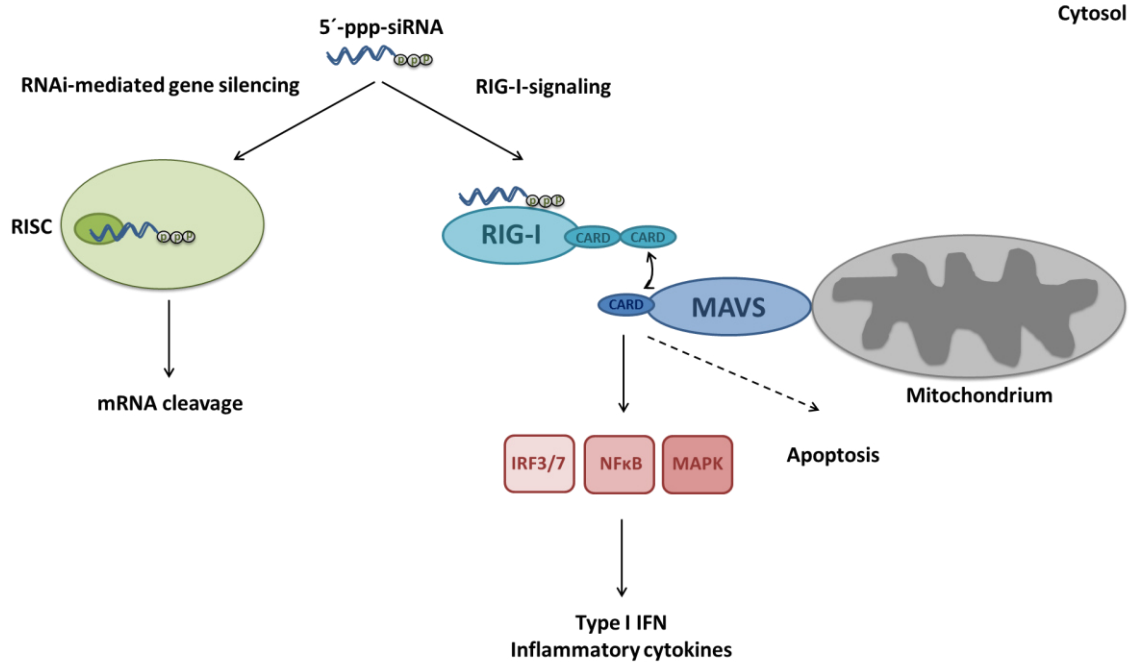
Figure 2: Dual activities of bifunctional 5'-ppp-siRNAs. Upon transfection into the cytosol, the 5'-ppp-siRNA can activate RIG-I, leading to NF-κB, IRF3/7 and MAPK signaling and the induction of intrinsic apoptosis. In addition, via incorporation into the RISC complex the 5'-ppp-siRNA leads to degradation of targeted mRNA with subsequent gene silencing (modified from Petrocca and Lieberman, 2008).

To what extent HCC is susceptible to such an immunotherapeutic approach is the subject of current research. Hou *et al.* (2014) revealed that RIG-I expression is positively correlated with the overall survival of HCC patients and serves as prognostic marker in regard to the effectiveness of an IFN-α-based therapy. Similar findings concerning the prognosis and the overall survival of patients suffering from HCC were made by Liu *et al.* (2015). In addition the same group demonstrated that increased levels of RIG-I minimized the proliferative and metastatic potential of the tumor by down-regulating the Matrix metalloproteinase-9 (MMP-9), a protein which is critically involved in the process of tumor migration and invasion (reviewed in Deryugina and Quigley, 2006). RIG-I is therefore not only suggested as prognostic marker, but also as therapeutic target (Hou *et al.*, 2014; Liu *et al.*, 2015). In this context, the intra-lesional administration of a synthetic RNA oligonucleotide-based RIG-I agonist is currently tested for its tolerability and safety in patients with injectable liver tumors or liver metastases in a phase I/II study (ClinicalTrials.gov, 2018c). In this regard the therapy´s efficacy and its immune mediated effector mechanisms in the liver related to its immune-privileged characteristics are still to be examined. Initial efforts have already been made by our group to show that a RIG-I-based immunotherapy is a promising therapeutic option for hepatocellular carcinoma (Funk, 2018; Lazić, 2017).

1.4.2.3   RIG-I agonists in comparison to TLR and STING agonists

Next to RIG-I other PRR were explored for the utility in the context of immunotherapy for cancer. In particular, Toll-like receptors (TLR) and cGas are also worth to be mentioned.

TLR sense pathogen-derived DNA, lipopolysaccharide and other pathogen-associated molecular patterns (reviewed in Takeda and Akira, 2004). TLR agonists are reported to have highly anti-tumoral potential (reviewed in Krieg, 2008) and some have already made it into clinical trials. In the context of HCC, TLR3 and TLR4 have been reported as valuable potential targets for anti-tumor therapy in preclinical studies (reviewed in Zou *et al.*, 2016). One critical point to consider is that some TLR are highly expressed on tissue of some tumor types and are under suspicion to promote tumor growth and migration (Kaczanowska *et al.*, 2013). TLR as therapeutic target in HCC remains controversial, as for example several studies demonstrated the anti-tumoral potential of TLR2 signaling in HCC (reviewed in Zou *et al.*, 2016). In contrast, Huang *et al.* (2012) demonstrated that knocking down TLR2 reduces metastasis formation *in vivo*. The same applies to TLR9 and TLR7: both proteins have been reported as being critically involved in tumor promotion as well as tumor inhibition (reviewed in Zou *et al.*, 2016). However, Tada *et al.* (2012) reported on a phase I/II clinical trial combining antigen pulsed DC with a TLR7 agonist for the treatment of patients suffering from HCC. The study revealed a tolerable safety profile, a TAA-specific T cell response but only a clinical response in one of five patients. The latter is maybe due to the advanced stage of HCC. To our knowledge, no further clinical trials in context of HCC therapy with TLR agonists have been reported so far.

The PRR cGas activates STING upon recognition of cytosolic DNA resulting in the induction of type I IFN. Regarding cancer therapy, STING agonists are controversial for anti-tumor therapy, but are shown to be effective in combination with checkpoint inhibitors for tumors unsusceptible to PD-1 blockade (Fu *et al.*, 2015). One major drawback in comparison to RLH is that some cancer types are impaired or even defective of STING signaling (reviewed in Baird *et al.*, 2017). Especially HCC tissue is reported to have decreased STING expression (reviewed in He *et al.*, 2017).

A major advantage of ppp-RNA-based RIG-I agonists in comparison to TLR and cGas agonists is the technical possibility to modify ppp-RNA as 5'-triphosphate-siRNA (5'-ppp-siRNA) thereby combining RIG-I activation and RNAi-mediated gene silencing in one molecule as already described in section 1.4.2.2. The therapeutic efficacy of bifunctional 5´-ppp-siRNAs has been successfully demonstrated for various tumor models. Studies revealed a more potent anti-tumoral effect mediated by bifunctional 5´-ppp-siRNA treatment as compared to solely inhibiting gene expression or activating RIG-I, respectively (Ellermeier *et al.*, 2013; Meng *et al.*, 2014; Petrocca and Lieberman, 2008; Poeck *et al.*, 2008). Lazić

Introduction

(2017) recently demonstrated that silencing c-Met, a well-known proto-oncogene in HCC, favors survival of liver tumor-bearing mice. The systemic treatment with bifunctional 5´-ppp-c-Met-siRNA even showed a stronger effect in the induction of tumor cell death than treatment with ppp-RNA alone.

2   Objectives

The long term goal of this project is to establish novel bifunctional 5´-ppp-siRNA-based therapeutics for the treatment of HCC that combine two modes of action: activation of the innate immune response via RIG-I signaling and interfering with pro-tumorigenic mechanisms by gene silencing via RNA interference.

During my Ph.D. studies I focused on the efficacy and mechanisms of action of RIG-I-based immunotherapy in murine HCC models. Following aims and questions were addressed:

1. Evaluation of RIG-I as target in HCC:
    - Is RIG-I expressed in human HCC tissue?
    - Is RIG-I signaling functional in human and murine HCC cell lines?
    - What is the functional outcome of RIG-I activation concerning viability and proliferation of tumor cells?
2. Establishment of orthotopic HCC mouse models
3. Assessment of the efficacy of RIG-I-based immunotherapy *in vivo*:
    - How do RIG-I ligands affect tumor growth and survival of tumor-bearing mice?
    - What are the immunological effects induced by this therapy?
        - Which types of immune cells are activated upon ppp-RNA therapy?
        - Which immune cells play a key role in the therapeutic setting?
        - Does the therapy induce an immunological memory?
    - What is the therapy´s toxicity profile?
    - Can therapeutic effects be improved in combination with checkpoint inhibitors?

3   Material

3.1   Instruments

Device name	Manufacturer
Blotting system	Bio-Rad, Germany
Cell culture CO_2 incubator (BD 6220)	Heraeus, Germany
Cell culture Laminar Flow	Thermo Scientific, Germany
Centrifuge (Multifuge 3L-R)	Thermo Scientific, Germany
Centrifuge (5424 and 5415R)	Eppendorf, Germany
ELISA reader (Mithras LB940)	Berthold Technologies, Germany
FACSCanto II	BD Bioscience, Germany
Gel electrophoresis system	peqlab, Germany
Lightcycler® 480 II	Roche, Germany
Microscope Axiovert25 and Axiovert200M	Zeiss, Germany
Microscope TCS SP5 II	Leica, Germany
NanoDrop® 2000c	Thermo Scientific, USA
pH meter	WTW, Germany
Power Pac Basic	Bio-Rad, Germany
Thermocycler T3	Biometra, Germany
Thermomixer	Eppendorf, Germany
Vortex Genie 2	Scientific Industries, Germany
Western blot analyzer (LAS4000 mini)	FujiFilm, Germany
ChemiDoc™Touch Imaging system	BioRad, Germany
Isofluran evaporator, VP series	Bioseb, USA/Canada
gentleMACS Dissociator	Miltenyi Biotec, Germany

3.2   Technical equipment

Name	Manufacturer
C Tubes (gentleMACS)	Miltenyi Biotec, Germany
Cannula Sterican, single-use, 0,40 x 20 mm	B. Braun, Germany
Cover glass	VWR, Germany
Gel blotting paper	Whatman Paper GmbH, UK
Immobilon®-P^{SQ} Transfer Membrane, PVDF, pore size 0.2 µm	Merck, Germany
Insulin syringe 0.3 ml (U-100), 29 G	Terumo, Germany
Insulin syringe 1 ml (U-40), 29 G	Terumo, Germany
Microscope slides Superfrost® Plus Menzel-	Thermo Fisher Scientific, USA

Material

Gläser	
Nitrocellulose membrane Amersham™-Hybond®-ECL™, pore size 0.45 µm	GE Healthcare, Germany
Rot®-PVDF, pore size 0.45 µm	Carl Roth, Germany
Scalpel (No. 22)	Feather, Japan
Suture material (Prolene 5-0)	Ethicon, USA
Syringes Omnifix, 1 ml	B. Braun, Germany

3.3 Chemicals and reagents

Chemical product	Manufacturer
Accutase	eBioscience, USA
Annexin Binding Buffer 10 x	eBioscience, USA
BD PharmLyse Lysis Buffer (10x concentrate)	BD Biosciences, Germany
Bromophenol blue	Sigma-Aldrich, Germany
Collagenase type I	Sigma-Aldrich, Germany
cOmplete™, Mini Protease Inhibitor Cocktail	Roche, Germany
DNase I recombinant	Roche, Germany
EDTA	Sigma-Aldrich, Germany
Ethanol p.a.	Sigma-Aldrich, Germany
Ethylenediaminetetraacetic acid (EDTA)	Sigma-Aldrich, Germany
FACSClean	BD Biosciences, Germany
FACSFlow	BD Biosciences, Germany
Glycerol	Carl Roth, Germany
In vivo-JetPEI™	Polyplus transfection, USA
Isoflurane-CP®	CP-Pharma, Germany
Isopropanol p.a.	Applichem, Germany
KAPA PROBE FAST Universal qPCR Master Mix	Peqlab Biotechnologie, Germany
Lipofectamine® RNAiMax Transfection Reagent	Thermo Fisher Scientific, USA
Methanol	Sigma-Aldrich, Germany
NP-40	Abcam, UK
PageRuler™ Plus Prestained Protein Ladder	Thermo Scientific, USA
Paraformaldehyde (PFA)	Merck, Germany
Phosphate Buffered Saline (PBS), (1x)	Lonza, Switzerland

Material

Powdered milk, blotting grade, low fat	Carl Roth, Germany
Propidium iodide	Immuno Tools, Germany
Sodium chloride	Merck, Germany
Sodium deoxycholate	Sigma-Aldrich, Germany
Sodium dodecyl sulfate (SDS)	Merck, Germany
Sodium orthovanadate	Sigma-Aldrich, Germany
Temgesic (Buprenorphin)	RB Pharmaceuticals, UK
Tris base	Carl Roth, Germany
Triton®-X 100	BioRad, Germany
Trypan blue	Sigma-Aldrich, Germany
Trypsin-EDTA(10x)	PAA, Austria
Tween® 20	Roth, Germany
β-Mercatptoethanol	Carl Roth, Germany

3.4 Cell culture

3.4.1 Cell lines

Name	Origin	Distributor
Hepa1-6	mouse	Kindly provided by Dr. Mike Helms, Sanofi, Germany
Hep-55.1C	mouse	CLS Cell Lines Service, Germany
RIL-175	mouse	Kindly provided by Prof. Tim Greten, Center for Cancer Research at the National Cancer Institute, USA and Nicolas Melin, Visceral and Transplantation Surgery, University of Bern, Switzerland
Hep3B	human	Kindly provided by Dr. Mike Helms, Sanofi, Germany
HepG2	human	Kindly provided by Dr. Mike Helms, Sanofi, Germany
HuH7	human	Kindly provided by Dr. Mike Helms, Sanofi, Germany

3.4.2 Media and supplements

Name	Manufacturer
Ciprofloxacin Kabi (200 mg/ml)	Fresenius Kabi, Germany
Dulbecco's modified Eagle's medium (DMEM), high glucose	Roth, Germany
Gibco™ Fetal bovine serum	Thermo Fisher Scientific, USA
Gibco™ Opti-MEM™ I Reduced Serum Media	Thermo Fisher Scientific, USA
L-glutamine (200 mM)	PAA, Austria

Lonza BioWhittaker™ Dulbecco's Modified Eagle's Medium with 4.5g L-Glucose per Liter, without L-Glutamine	Lonza, Switzerland
Lonza BioWhittaker™ RPMI 1640 without L-Glutamine	Lonza, Switzerland
Phosphate Buffered Saline (PBS), (1x)	Lonza, Switzerland

Plastic material for cell culture was purchased from BD Bioscience (Germany), Corning (USA), Eppendorf (Germany), Greiner Bio-One (Germany) or Sarstedt (Germany).

3.5 Kits

Name	Manufacturer
DC Protein Assay	BioRad, Germany
HiScribe™ T7 Quick High Yield RNA Synthesis Kit	New England Biolabs, Germany
Klenow Fragment, exo– (5 U/µL)	Thermo Fisher Scientific, USA
Oligo Clean-Up and Concentration Kit (Cat. 34100-NB)	Norgen Biotek Corp., Canada
RevertAid H Minus First Strand cDNA Synthesis Kit	Thermo Fisher Scientific, USA
RNA Clean-Up and Concentration Kit (Cat. 43200-NB)	Norgen Biotek, Canada
SuperSignal™ West Femto Maximum Sensitivity Substrate	Thermo Fisher Scientific, USA
Total RNA Kit, peqGOLD	Peqlab Biotechnologie, Germany

3.6 Antibodies

3.6.1 FACS analysis

Specificity	Fluorochrome	Clone	Isotype	c [mg/ml]
Mouse CD103	APC	2E 7	Hamster IgG	0.2
Mouse CD11c	PerCP	N418	Hamster, IgG	0.2
Mouse CD178	PE	MFL3	Hamster, IgG	0.2
Mouse CD19	PE/Cy7	6D5	Rat IgG2a, κ	0.2
Mouse CD19	FITC	1D3	Rat IgG2a, κ	0.5
Mouse CD25	FITC	PC61	Rat IgG1, λ	0.5
Mouse CD279	APC	10F.9G2	Rat IgG2b, κ	0.2

Material

Mouse CD3	APC	17A2	Rat IgG2b, κ	0.2
Mouse CD3	PB	17A2	Rat IgG2b, κ	0.5
Mouse CD4	PE/Cy7	RM4-5	Rat IgG2a, κ	0.2
Mouse CD4	FITC	RM4-5	Rat IgG2a, κ	0.5
Mouse CD45	PB	30-F11	Rat IgG2b, κ	0.5
Mouse CD45	PE	30-F11	Rat IgG2b, κ	0.2
Mouse CD69	FITC	H1.2F3	Hamster IgG1, λ	0.5
Mouse CD8	PerCP	53-6.7	Rat IgG2a,κ	0.2
Mouse CD8	APC	53-6.7	Rat IgG2a, κ	0.2
Mouse CD86	FITC	GL1	Rat IgG2a, κ	0.5
Mouse CD95	PE/Cy7	Jo2	Hamster IgG2, λ	0.2
Mouse F4/80	APC	BM8	Rat IgG2a, κ	0.2
Mouse Gr-1	PE	RB6-8C5	Rat IgG2b, κ	0.2
Mouse H-2K^b	FITC	AF6-88.5	Mouse IgG2a, κ	0.5
Mouse I-A/I-E	PE	M5/11.15.2	Rat IgG2b, κ	0.2
Mouse NK-1.1	PerCP	PK136	Mouse IgG2a, κ	0.2
Mouse/human CD11b	PE/Cy7	M1/70	Rat IgG2b, κ	0.2
Mouse/rat Foxp3	PE	FJK-16s	Rat IgG2a, κ	0.5

Annexin V, APC conjugate was purchased from Immuno Tools (Germany).

All antibodies and their respective IgG isotype controls were purchased from BioLegend (USA), BD Pharmingen (USA), BD Biosciences (USA) or eBioscience (USA). The viability dye Fixable Viability Dye eFluor® 780 was purchased from eBioscience (USA). TruStain FcX™ (anti-mouse CD16/32) antibody was purchased from BioLegend (USA) and used in accordance with the manufacturer´s instructions.

3.6.2   Functional assays

Specifity	Clone	Isotype	Function
Mouse CD8α	YTS 169.4	Rat IgG2b	Depletion
Mouse CD4	GK1.5	Rat IgG2b	Depletion
Mouse NK-1.1	PK136	Mouse IgG2a	Depletion
Mouse CD279	RMP1-14	Rat IgG2a	Blocking
Mouse CD95	Jo2	Hamster IgG$_2$, λ	Activation

In vivo antibodies and IgG isotype controls were purchased from BioXcell (USA). Anti-mouse CD95 antibody and respective IgG isotype control were purchased from BD Pharmingen (USA).

3.6.3   Western blot analysis

Specificity	Clone	Isotype	Modification	c [µg/ml]
Human, mouse, rat RIG-I	D-12	mAb IgG1	None	200
Human, mouse RIG-I	Alme-1	mAb IgG1	None	1000
Human, mouse, β-Actin	C4	mAb	HRP	200

All primary antibodies were purchased from Santa Cruz Bioctechnology (USA) and Adipogen Life Sciences (Switzerland), respectively. As secondary antibody goat anti-mouse IgG-HRP from Santa Cruz Bioctechnology (USA) was used.

3.7   Software

Software name	Provider
FlowJo 10.0	FloJo LLC, USA
GraphPad Prism 5.0	GraphPad Software, USA
Image Lab™	BioRad, Germany
ImageJ	Wayne Rasband and Cuertis Rueden

4 Methodology

4.1 Animal experiments

4.1.1 Animals

C57BL/6JRi mice were purchased from Janvier Labs, France. *Ifnar1r*^{-/-} and *Mavs*^{-/-} mice were kindly provided by Ulrich Kalinke (Institute for Experimental Infection Research, TWINCORE, Centre for Experimental and Clinical Infection Research, Hannover Medical School). NOD.Cg-Prkdc[scid] Il2rg[tm1Wjl]/SzJ (NOD-*scid IL2Rγ*[null], NSG) mice were provided by the animal facility´s own breeding.

All animal studies were approved by the local regulatory agency (Regierung von Oberbayern, Munich, Germany; experimentation application number 55.2-1-54-2532-52-2013).

4.1.2 *In vivo* experiments

4.1.2.1 Orthotopic tumor implantation

For orthotopic tumor implantation, cells were harvested with accutase and washed twice with PBS. Cell number was adjusted as follows:

- RIL-175: 5×10^5 cells/20 µl PBS
- Hep-55.1C: 2×10^6 cells/20 µl PBS
- Hepa1-6: 1×10^6 cells/20 µl PBS.

20 µl cell suspension were injected into the left liver lobe using a Hamilton syringe. Mice were sutured with Prolene 5 - 0 from Ethicon.

Surgical procedure was performed under Isoflurane anaesthesia. For peri-operative pain management 0.125 mg/kg Buprenorphin in NaCl 0.9 % were injected before and 24 h and 48 h after surgery.

4.1.2.2 Subcutaneous tumor induction

For subcutaneous tumor induction cells were prepared as for orthotopic tumor implantation (see section 4.1.2.1). 5×10^5 RIL-175 cells were injected subcutaneously with a 29 Insulin syringe into the flank of mice.

4.1.2.3 CT imaging

CT imaging of orthotopic liver tumors was performed in collaboration with Prof. Kirsten Lauber and Dr. Benjamin Stegen, Department of Radiation Oncology, LMU Munich. For this purpose, mice were anesthetized with isoflurane. Iodine was used as contrast agent and was injected i.v. prior to imaging.

4.1.3   *Ex vivo* analysis

4.1.3.1   Single cell preparation from tumor and spleen

For single cell preparation from tumors, tissue was minced and transferred to a gentleMACS™ C Tube containing a DNase-Collagenase-mix. Tissue preparation was performed according to the protocol of the Tumor dissociation Kit, mouse from Miltenyi Biotec using a DNAse-Collagenase-mix instead of the enzyme mixes provided by the kit.

DNase-Collagenase-mix:
1 mg/ml Collagenase Type I
100 U/ml DNase I
in RPMI 1640

For single cell preparation from spleen, tissue was mashed through a 40 µm cell strainer and flushed with 10 ml 10 % FBS in PBS. The cell suspension was centrifuged at 400 g for 5 min at RT. Cells were directly used for lysis of erythrocytes using the BD Pharm Lyse™ Buffer according to the manufacturer´s instructions.

4.2   Cell culture

Tumor cells were cultured in DMEM medium supplemented with 10 % FBS and 10 µg/ml ciprofloxacin under the following conditions:

- 37°C
- 10 % CO_2
- 95 % humidity.

4.3   Immunological methods

4.3.1   Enzyme-linked immunosorbent assay

For the detection of IP-10 (CXCL10) in the supernatant or plasma an enzyme-linked immunosorbent assay (ELISA) was performed. For murine samples the CXCL10 ELISA Kit from R&D Systems, for human samples the OptEIA™ Human IP-10 ELISA from BD Biosciences was used. The assay was performed according to the manufacturer´s instructions except that only half of the volume of the reagents specified by the manufacturer was used. Samples were diluted.

4.3.2   Flow cytometry

4.3.2.1   Staining of extra- and intracellular proteins

Cells were washed with 1 ml FACS buffer and centrifuged (5 min, 400 g, RT). Cells were incubated with FACS buffer containing a live-dead-stain and diluted antibodies for 20 min at

RT. Subsequently cells were washed with 1 ml FACS buffer and centrifuged (5 min, 400 g, RT). Samples were directly used for flow cytometric analysis or prepared for intracellular staining using the Foxp3/Transcription Factor Staining Buffer Set (eBioscience) according to the manufacturer´s instructions.

All antibodies were diluted 1:200 for flow cytometry. Except anti-FoxP3 antibody was diluted 1:40. Respective IgG isotypes served as control. For discrimination of living and dead cells the Fixable Viability Dye eFluor® 780 (eBioscience) was used 1:1000. For *ex vivo* analysis, cells were incubated with TruStain FcX™ antibody (BioLegend) prior to staining according to the manufacturer´s instructions. For the analysis of FasL, FACS buffer was supplemented with 1 x cOmplete™, Mini Protease Inhibitor (Roche).

<u>FACS buffer:</u>
0.5 g sodium azide
2 ml EDTA (0.5 M)
5 ml FBS
ad 500 ml PBS

4.3.2.2 Annexin V/PI staining
For Annexin V staining cells were prepared as recommended by the manufacturer. 1 µl PI (250 ng/ml) was added directly before analysis.

4.3.3 Immunhistochemistry
For immunohistochemical analysis of human HCC tissue 239 human tissue microarrays (TMA) were investigated: 179 samples were provided by PD Dr. Enrico de Toni, Liver Center, LMU Munich and 60 by the Department of Pathology, LMU Munich. Immunohistochemical preparation of human TMA was performed by Prof. Doris Mayr, Department of Pathology, LMU Munich. Analysis was performed by Dr. Lars König, Division of Clinical Pharmacology, LMU Munich. For the detection of RIG-I mAb IgG1, clone Alme-1 was used. Analyzed were two biopsy punches per patient from different tumor regions.

4.3.4 Western blot analysis
4.3.4.1 Preparation of protein lysates
To extract proteins, cells were lysed with supplemented RIPA or NP-40 buffer. Whole cell lysates were centrifuged (20 min, 16,000 rpm, 4°C) in a benchtop centrifuge and supernatants were collected. The concentration of proteins was determined using the DC Protein Assay from BioRad. Protein lysates were either stored at -20°C or directly used for western blot analysis.

RIPA buffer:

150 mM sodium chloride

1.0 % (v/v) Triton X-100

0.5 % (w/v) sodium deoxycholate

0.1 % (w/v) SDS

50 mM Tris, pH 8.0

NP-40 buffer:

150 mM sodium chloride

1.0 % (v/v) NP-40

50 mM Tris pH 8.0

Supplements:

1 x proteinase inhibitors (cOmplete™, Mini Protease Inhibitor Cocktail, Roche)

4.3.4.2   SDS-PAGE

30 µg of whole proteins were mixed with appropriate amount of 6 x Laemmli loading buffer and denaturated at 95°C for 5 min. Samples were loaded on a SDS gel (10-12 %) and separated by an applied voltage of 100 V for 1.5 h. The PageRuler™ Plus Prestained Protein Ladder (Thermo Fisher Scientific) was used as reference.

Laemmli buffer (6 x):

7 ml Tris (0.5 M)

1 g SDS

3 ml glycerol

1.2 mg bromophenol blue

680 µl β-mercatptoethanol

Running buffer:

248 mM Tris

14 mM SDS

1.92 M glycine

4.3.4.3   Protein transfer

Proteins were transferred from the SDS gel to a nitrocellulose membrane or a PVDF membrane, which was previously activated in methanol, applying 250 mA for 1.5 h. Subsequently, the membrane was rinsed with distilled water. It was then washed three times for 10 min each in TBS-T. The membrane was incubated rotating in blocking buffer for 1 h at

RT or at 4°C over night. The primary antibody (diluted in blocking buffer) was incubated over night at 4°C rotating. Afterwards, the membrane was incubated in TBS-T for 10 min at RT. This step was repeated two times. The secondary antibody (diluted in blocking buffer) was incubated for 60 min at RT rotating. The membrane was incubated in TBS-T for 10 min at RT three times each. Afterwards it was incubated in TBS for another 10 min. The antibody signal was developed using the SuperSignal™ West Femto Maximum Sensitivity Substrate (Thermo Fisher Scientific) according to the manufacturer´s instructions. The analysis of protein bands was performed using the western blot analyzer LAS4000 mini (FujiFilm) and the ChemiDoc™Touch Imaging system (BioRad), respectively.

Transfer buffer (20 x):
198 mM Tris
2 M glycine

TBS:
50 mM Tris
150 mM NaCl
HCL (ad pH 7.6)

Washing buffer (TBS-T):
TBS 1 x
0.5 % (v/v) Tween 20

Blocking buffer:
5 % (w/v) powdered milk in TBS-T

4.4   Molecular biological methods

4.4.1   RNA isolation
RNA from cultivated cells and tissue was isolated using the Total RNA Kit from Peqlab according to the manufacturer´s instructions.

4.4.2   cDNA synthesis
cDNA was synthesized using the RevertAID™ First strand cDNA Synthesis kit (Thermo Fisher Scientific) according to the manufacturer´s instructions.

4.4.3   Relative quantification of mRNA levels
Relative mRNA expression levels were analyzed via quantitative real time-PCR (qRT-PCR) using the KAPA PROBE FAST qPCR Kit (Peqlab). Probes required for qRT-PCR were

purchased from Roche and oligonucleotides were therefore designed with respect to the Roche Library.

Probes and sequences of the oligonucelotides used are listed below:

Gene	Species	Forward (5´ -> 3´)	Reverse (5´ -> 3´)
ifnb1	human	CTT TGC TAT TTT CAG ACA AGA TTC A	GCC AGG AGG TTC TCA ACA AT
	mouse	GCA GAA CTG GAA CAG GTC GT	TGT TCG AAG TCC GGG ATG
ddx58	mouse	CAC AGT GTC AAT GCC TCC AA	TTG CTG ACC CAG AAG ATG G
actb	human	CCA ACC GCG AGA AGA TGA	CCA GAG GCG TAC AGG GAT AG
	mouse	CTA AGG CCA ACC GTG AAA AG	ACC AGA GGC ATA CAG GGA CA

All oligonucleotides were purchased from Eurofins Genomics.

For each sample a reaction mixture was prepared as follows:

Reagent	Volume [µl]
KAPA PROBE FAST Universal qPCR Master Mix (2 x)	5.0
Primer forward (100 γM)	0.2
Primer reverse (100 γM)	0.2
Probe 10 x	0.1
H_2O_{ddest}	ad 10

2 µl cDNA diluted 1:2 in H_2O_{ddest} were added. Expression of mRNA was assessed using the LightCycler® 480 (software Version 1.5) from Roche and the detection format 'monocolor hydrolysis probes'.

Program settings are described in the table below:

Number of cycles	Temperature [°C]
1	95
45	60
1	40

Relative mRNA expression levels were calculated taking the primer efficiency, prior calculated via a relative standard curve, into account.

4.4.4 *In vitro* transcription

The respective DNA template for generating the 5´-triphosphate-RNA (ppp-RNA) was purchased from Eurofins Genomics with the following sequence (CO4hp): 5´-GCG CTA TCC AGC TTA CGT A GAGCTC T ACG TAA GCT GGA TAG CGC TAT   AGT GAG TCG TAT TA-3´. It was annealed to a T7 promoter primer with the following sequence:

5´-TAA TAC GAC TCA CTA TA-3´. A double-stranded DNA-template was generated using the Klenow Polymerase from Thermo Fisher Scientific according to the manufacturer´s instructions.

Alternatively, the sense and antisense CO4hp-template strands were annealed to form the double-stranded DNA-template.

The ppp-RNA was generated via *in vitro*-transcription (IVT) using the HiScribe™ T7 Quick High Yield RNA Synthesis Kit from New England Biolabs GmbH according to the manufacturer´s instructions with a template concentration of 1 µM.

The RNA was purified using the RNA Clean-Up and Concentration Kit from Norgen Biotek according to the manufacturer´s instructions.

4.4.5 Transfection of RNA

One day prior to transfection cells were seeded in appropriate culture dishes in cell culture medium. On day of transfection medium was changed to transfection medium. Cells were transfected with RNA using Lipofectamin® RNAiMax (Thermo Fisher Scientific) according to the manufacturer´s instructions. For transfection of 40 nM RNA 3 µl transfection reagent were used. The same N/P-ratio was used for higher or lower concentrations.

Cells were either transfected with ppp-RNA, generated as described in section 4.4.4 or with the double-stranded control RNA (OH-RNA) purchased from Eurofins Genomics with the following sequence: 5´-GCG CUA UCC AGC UUA CGU A-3´ with and without dTdT-3´modification.

Transfection medium:
DMEM
L-Glut (2 mM)
1 % (v/v) FBS

4.5 Statistical analysis

Statistical analysis was performed using GraphPad PRISM 6.0 from GraphPad Software (USA). *In vitro* data are presented as mean and standard deviation (SD). *In vivo* data are presented as mean and standard error of the mean (SEM). Unpaired data were analyzed via ordinary one-way ANOVA followed by Tukey´s multiple comparisons tests and unpaired t test with Welch's correction, respectively. Paired data were analyzed using a paired t test. Data were considered statistically significant if $p < 0.05$. Survival analysis was depicted as Kaplan-Meier estimator. To compare survival distributions a log-rank test was performed.

5 Results

The cytosolic helicase RIG-I serves as potential target for the development of an immunotherapy for the treatment of HCC (section 1.4.2). In order to investigate this hypothesis more closely in the context of this work, RIG-I expression first was assessed in murine and human HCC cell lines, as well as in human HCC tissue cores. The protein´s functionality was further examined *in vitro*. After having established two orthotopic mouse models of HCC, the efficacy of the ppp-RNA-based immunotherapy and its immune-mediated effector functions were investigated *in vivo.* The underlying results are described in the following.

5.1 RIG-I expression and regulation in human and murine HCC

In order to evaluate RIG-I as target for a ppp-RNA-based immunotherapy in HCC, a set of 239 tissues microarrays (TMA) of human HCC cores and three human (Huh7, Hep3B, HepG2) as well as three murine cell lines (RIL-175, Hep-55.1C, Hepa1-6) were investigated concerning RIG-I expression and regulation.
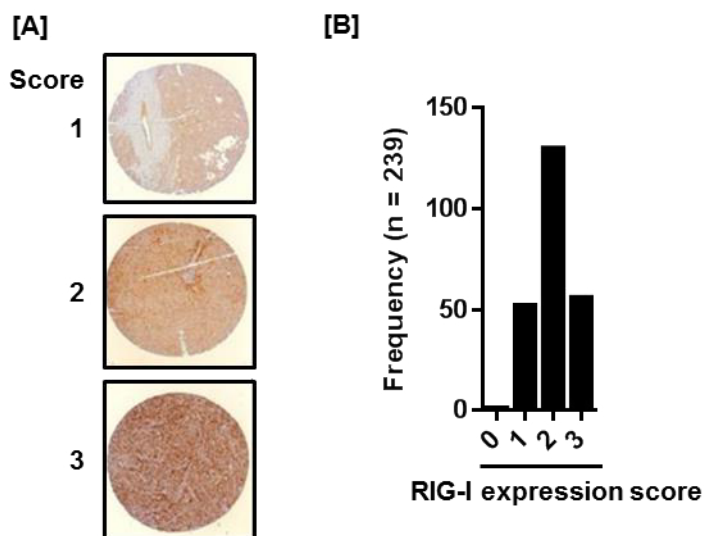
Figure 3: RIG-I is expressed in human HCC tissue. RIG-I expression in tissue microarrays of 239 human HCC samples was analyzed via immunohistochemical staining. [A] RIG-I expression levels were defined through an expression score as depicted. [B] Frequency of RIG-I expression was determined using the RIG-I expression score (0 = unstained, 1 = low expression, 2 = moderate expression, 3 = high expression). Analysis was performed in collaboration with Prof. Doris Mayr, Department of Pathology, LMU Munich.

The TMA of human HCC biopsies were investigated for RIG-I expression via immunohistochemical staining and the strength of expression was classified through a score from 1 to 3 (0 = unstained/no expression, 1 = low expression, 2 = moderate expression, 3 = high expression). 52 TMA were scored as 1, 130 as 2, 56 as 3 and only a single sample did not show any expression (Figure 3). RIG-I expression was confined to tumor cells rather than fibrotic tissue and the majority of samples exhibited moderate to strong RIG-I expression.

Results
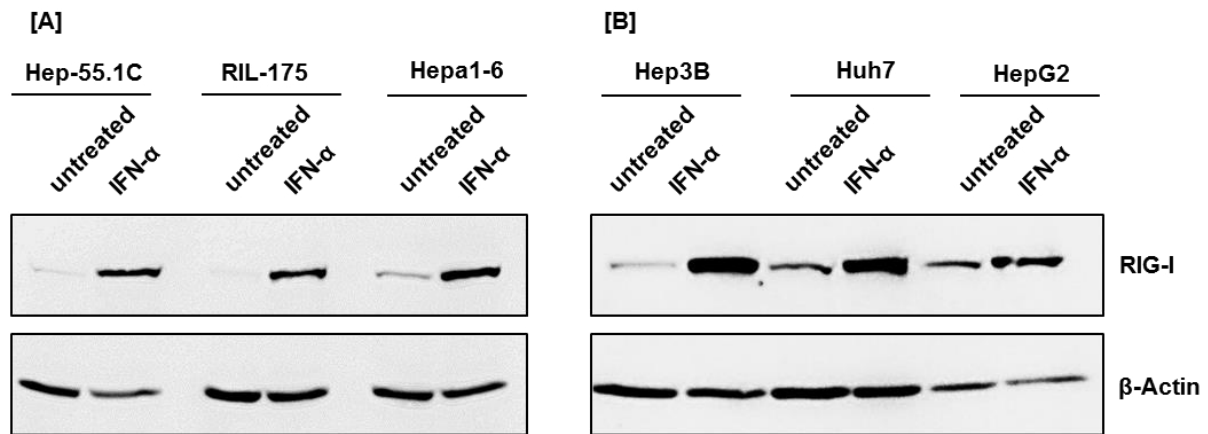
Figure 4: RIG-I is inducible in murine and human HCC cell lines. [A] Murine (Hep-55.1C, RIL-175, Hepa1-6) and [B] human (Huh7, Hep3B, HepG2) cells were stimulated with 1000 U/ml IFN-α for 48 h hours. RIG-I expression was assessed via western blot analysis. Untreated condition served as reference. Depicted is one representative experiment out of three.

In order to test whether murine (Hep-55.1C, RIL-175, Hepa1-6) and human HCC (Huh7, Hep3B, HepG2) cell lines express RIG-I, protein levels were analyzed via western blot analysis in unstimulated as well as INF-α stimulated cells. Baseline expression levels of RIG-I were low, but readily induced by IFN stimulation (Figure 4). Next, RIG-I expression was studied in HCC cells via qRT-PCR and western blot after treatment with ppp-RNA and a respective control RNA (OH-RNA) (Figure 5). A specific upregulation of RIG-I was observed in murine and human HCC cell lines after transfection with ppp-RNA, with the exception of Huh7 cells, indicative of a positive type I IFN-mediated feed-back loop (Figure 5).

Results
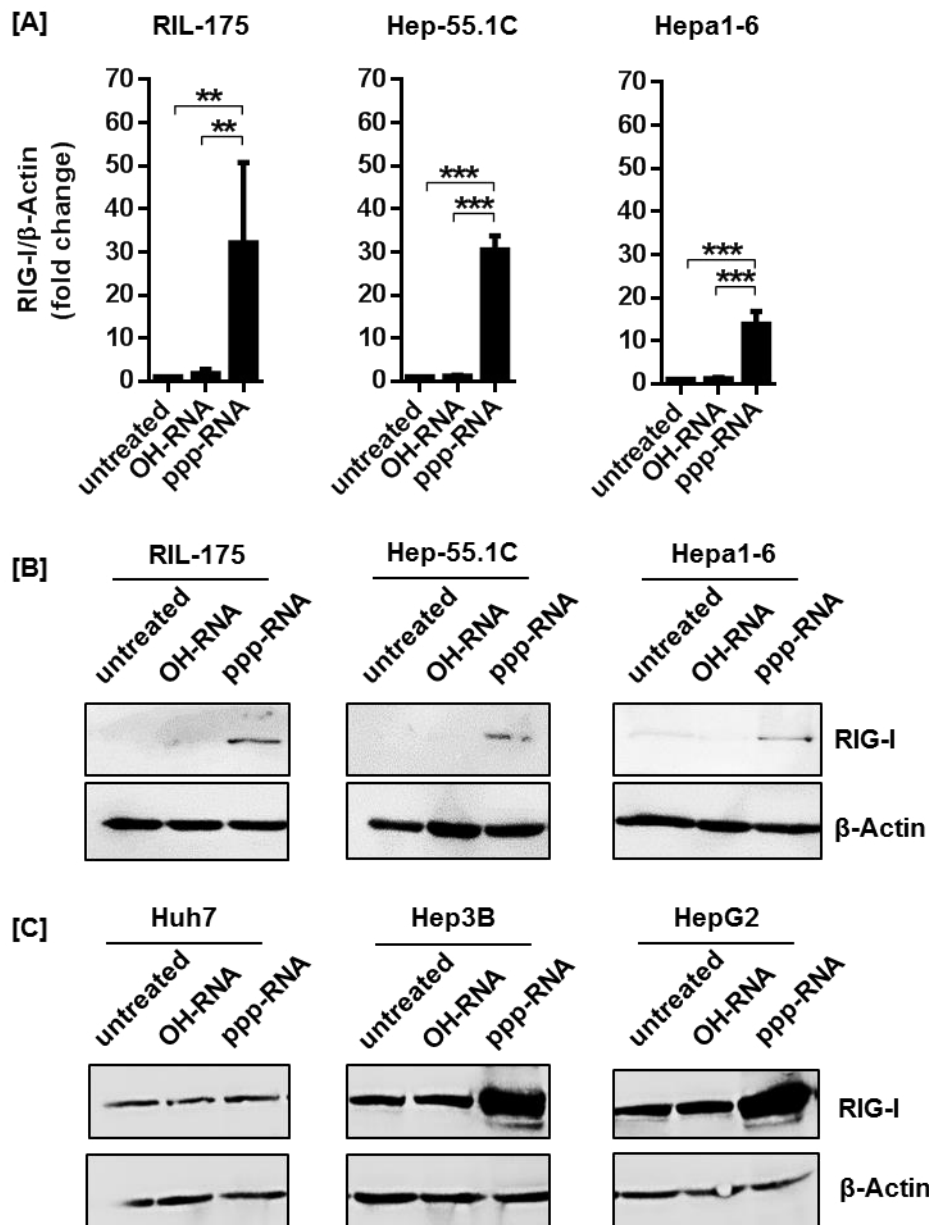
Figure 5: ppp-RNA treatment leads to RIG-I upregulation in murine and human HCC cells. Murine (RIL-175, Hep-55.1C, Hepa1-6) and human (Huh7, Hep3B, HepG2) HCC cells were transfected with 40 nM ppp-RNA and control RNA (OH-RNA), respectively. Untreated conditions served as additional controls. RIG-I expression [A] on mRNA level was investigated 24 h after transfection by qRT-PCR and [B], [C] on protein level 48 h after transfection via western blot analysis. qRT-PCR results are shown as mean of three experiments. Error bars represent standard deviation. Statistical analysis was performed via ordinary one-way ANOVA and Tukey´s multiple comparisons tests. Asterisks indicate p-values: ** < 0.01; *** < 0.001. Western blot analysis represents one representative experiment out of three.

5.2 Functional consequences of RIG-I activation in murine and human HCC cell lines

As the treatment with ppp-RNA of murine and human HCC cells induced RIG-I expression *in vitro* (Figure 4 and Figure 5), functional consequences of the activation of this signaling pathway were investigated. To this end, downstream effects like MHC-I upregulation, IFN-β induction, IP-10 secretion and cell death were analyzed. MHC-I was upregulated upon ppp-RNA stimulus in RIL-175 and Hep-55.1C cells, but not in Hepa1-6 cells, whereas IFN-β and IP-10 were induced in all three murine cell lines. Furthermore, ppp-RNA treatment induced tumor cell death (Figure 6). Similar effects of ppp-RNA treatment were observed for human Hep3B and Huh7 cells: the transfection of cells with ppp-RNA led to the upregulation of HLA-I and IFN-β and the secretion of IP-10. In addition, it significantly reduced tumor cell viability (Figure 7).

Results

RIL-175   Hep-55.1C   Hepa1-6

[A] MFI MHC-I (normalized to IgG)

[B] IFN-β/β-Actin (fold change)

untreated   OH-RNA   ppp-RNA

[C] IP-10 [pg/ml]

RIL-175   Hep-55.1C   Hepa1-6

[D] Viability [%] normalized to untreated

untreated   20 nM   40 nM   20 nM   40 nM
OH-RNA   ppp-RNA
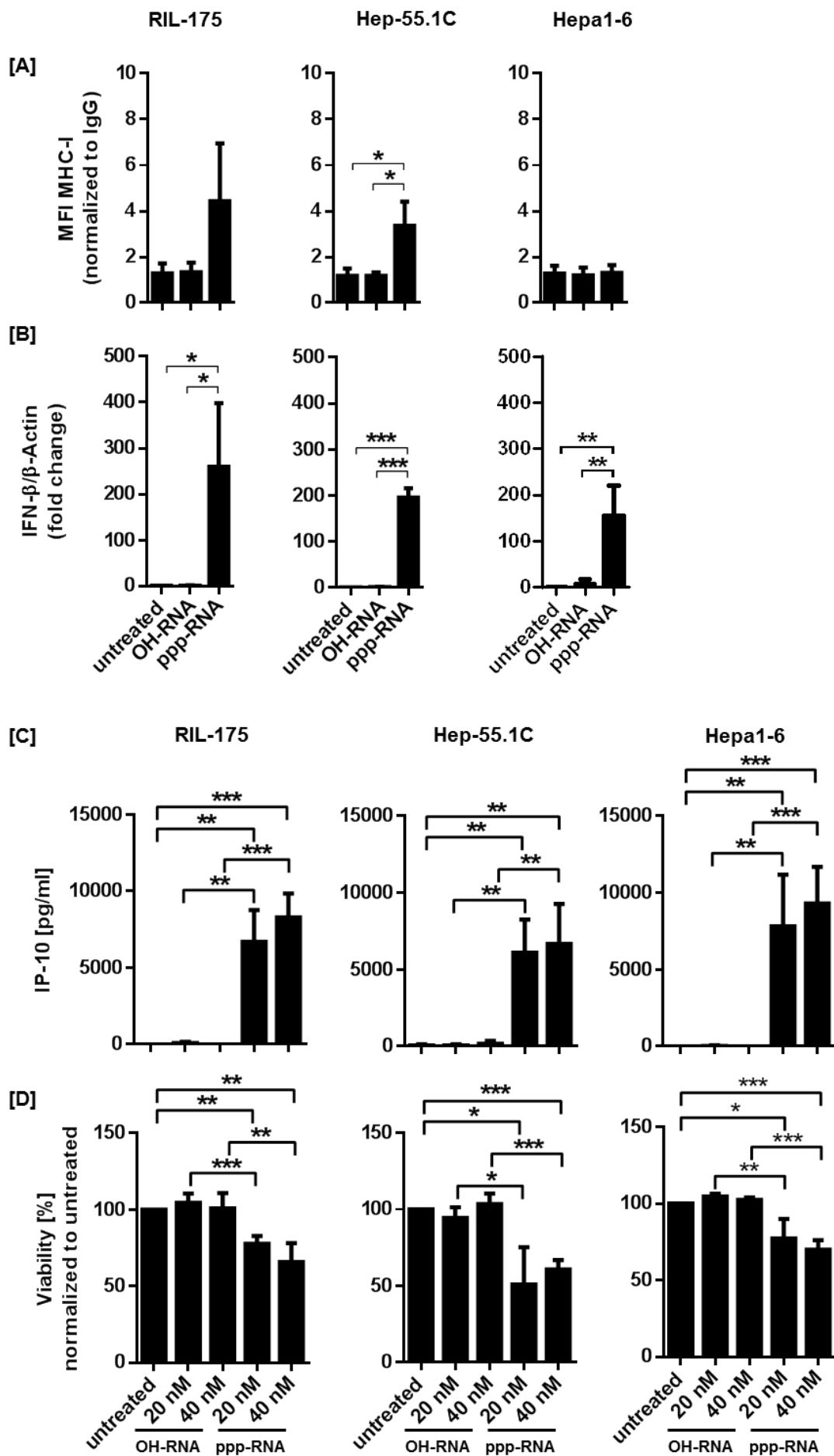
Results

Figure 6: RIG-I signaling is functional in murine HCC cells. RIL-175, Hep-55.1C and Hepa1-6 cells were transfected with 40 nM ppp-RNA and 40 nM control RNA (OH-RNA), respectively. Untreated conditions served as additional controls. [A] Upregulation of MHC-I was analyzed 48 h after transfection via flow cytometry. [B] Induction of IFN-β expression was assessed 24 h after transfection on mRNA level by qRT-PCR. [C] Secretion of IP-10 was detected 48 h after transfection in the cell culture supernatant via ELISA. [D] Cell death was analyzed 48 h after transfection via Annexin V/PI staining and flow cytometry. Viable cells were defined as double negative population. Results are shown as mean of three experiments. Error bars represent standard deviation. Statistical analysis was performed via ordinary one-way ANOVA and Tukey´s multiple comparisons tests. Asterisks indicate p-values: *<0.05; ** < 0.01; *** < 0.001.

Figure 7: RIG-I signaling is functional in human HCC cells. Huh7 and Hep3B cells were transfected with 40 nM ppp-RNA or 40 nM control RNA (OH-RNA). Untreated conditions served as additional controls. [A] Upregulation of MHC-I was analyzed 48 h after transfection via flow cytometry. [B] Induction of IFN-β expression was assessed 24 h after transfection on mRNA level by qRT-PCR. [C] Secretion of IP-10 was detected 48 h after transfection in the cell culture supernatant via ELISA. [D] Cell death was analyzed 48 h after transfection via Annexin V/PI staining and flow cytometry. Viable cells were defined as double negative population. Results are shown as mean of three experiments. Error bars represent standard deviation. Statistical analysis was performed via ordinary one-way ANOVA and Tukey´s multiple comparisons tests. Asterisks indicate p-values: *< 0.05; ** < 0.01; *** < 0.001.

5.3 Establishing orthotopic HCC *in vivo* models

In order to investigate the therapeutic effect of ppp-RNA-based immunotherapy, orthotopic murine HCC models were established. To this end, Hep-55.1C, RIL-175 or Hepa1-6 cells were injected into the left liver lobe of C57BL/6 mice. A tumor growth analysis was performed based on CT imaging and survival of tumor-bearing mice was monitored over 60 days. Injection of Hep-55.1C and RIL-175 cells into the liver led to steady tumor cell growth and resulted in tumor-related death, whereas Hepa1-6 cells only led to the establishment of a liver tumor in 3 out of 7 mice (Figure 8). Unreliable tumor take of Hepa1-6 cells was surprising, as this is a well-described HCC *in vivo* model in the literature (He *et al.*, 2016; Kuang *et al.*, 2013; Ma *et al.*, 2014; Rao *et al.*, 2016).
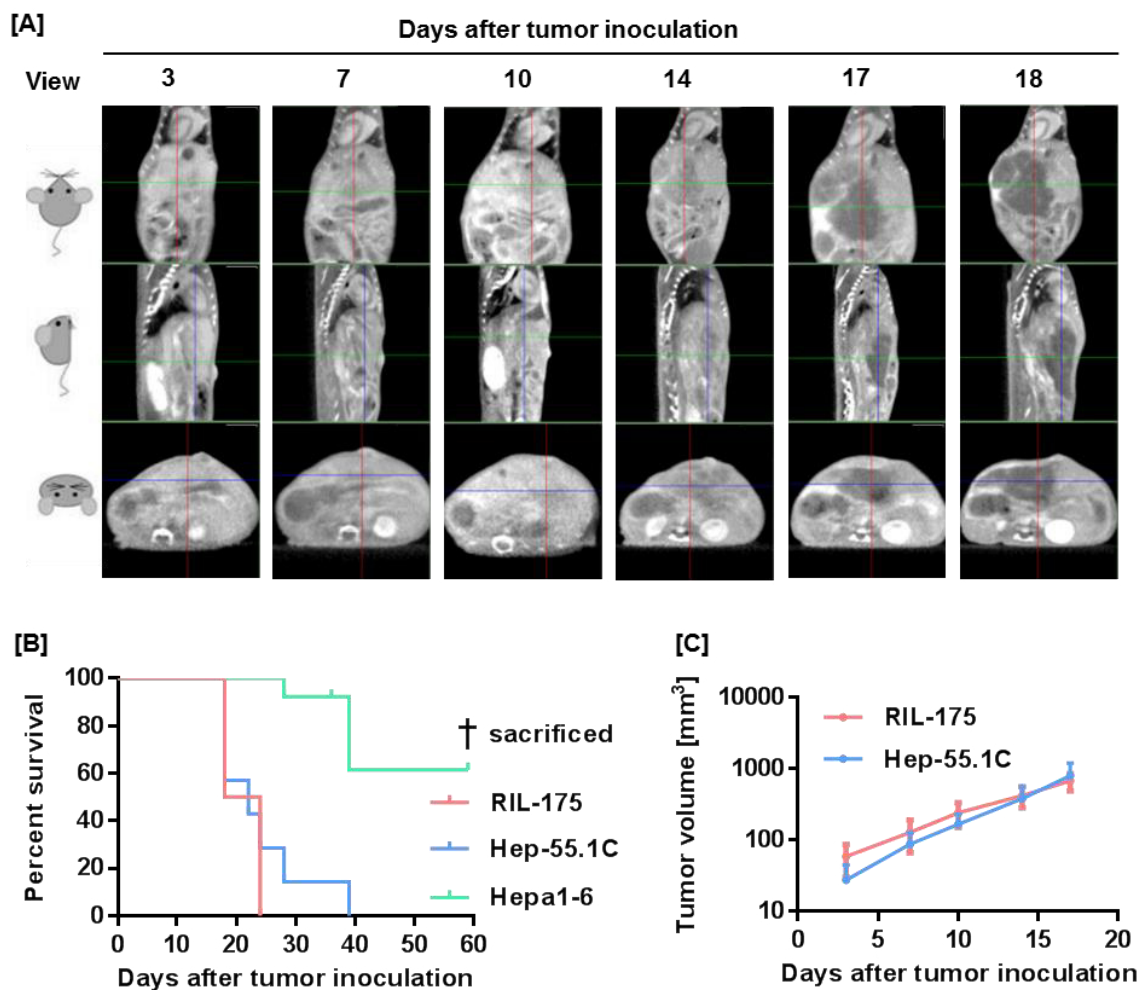
Figure 8: RIL-175 and Hep-55.1C cells are suitable for HCC *in vivo* studies. RIL-175 (n = 6), Hep-55.1C (n = 7) or Hepa1-6 cells (n = 7) were orthotopically transplanted into the left liver lobe of C57BL/6 mice. [A] Exemplarily shown is the CT-based imaging of a RIL-175 tumor on indicated days after tumor inoculation. [B] Survival of mice with induced tumors is depicted as Kaplan-Meier curve. [C] Orthotopic tumor growth was monitored via CT and tumor volumes were calculated using ImageJ. CT analysis was performed in collaboration with Prof. Kirsten Lauber and Dr. Benjamin Stegen, Department of Radiation Oncology, LMU Munich.

5.4   *In vivo* ppp-RNA-based immunotherapy of HCC

After having established two murine orthotopic HCC *in vivo* models (Hep-55.1C and RIL-175 cells) (Figure 8), the *in vivo* efficacy of RIG-I-based immunotherapy was assessed.

5.4.1   Therapeutic efficacy

In order to address how systemic ppp-RNA treatment affects tumor growth and survival of tumor-bearing mice, RIL-175 or Hep-55.1C cells were orthotopically induced in C57BL/6 mice. After 5 days for tumor engraftment, mice were treated every 3-4 days with i.v. injections of ppp-RNA or a respective control RNA (OH-RNA). Survival of mice was monitored for up to 100 days. Therapy with ppp-RNA significantly prolonged median survival in the RIL-175 tumor model to 46 days as compared to 24 or 25 days in the control groups. In contrast, mice bearing Hep-55.1C-tumors did only marginally benefit from ppp-RNA therapy in comparison to untreated mice, but not in comparison to mice injected with control RNA (OH-RNA) (Figure 9, Table 1, Table 6).
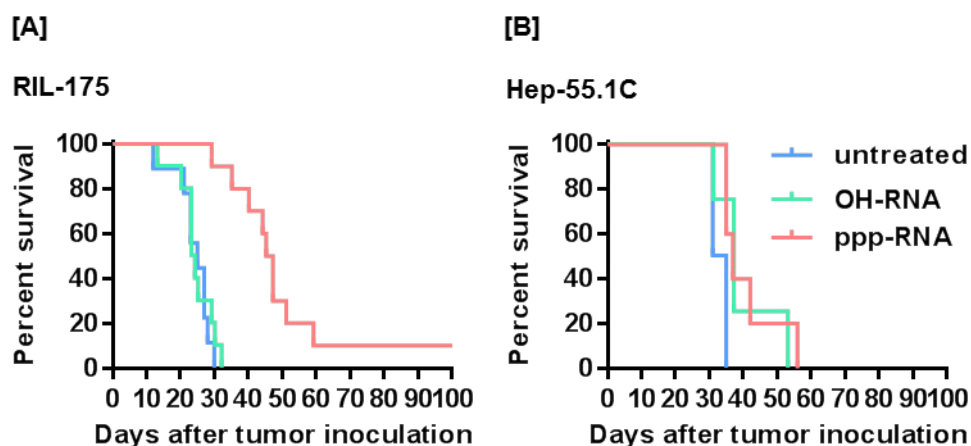
Figure 9: ppp-RNA immunotherapy significantly prolongs survival of RIL-175 tumor-bearing mice. [A] RIL-175 or [B] Hep-55.1C cells were induced orthotopically in the left liver lobe of C57BL/6 mice. Mice were treated with 50 µg ppp-RNA complexed to in vivo-jetPEI® or control RNA (OH-RNA) on days 5, 9, 12, 16, 19 and 23 after tumor inoculation via i.v. injection or left untreated. Survival was monitored over 100 days and is depicted as Kaplan-Meier curve. P-values were calculated performing a log-rank test and are listed in Table 1 (RIL-175 tumor-bearing mice: n (untreated) = 9; n (OH-RNA) = 10; n (ppp-RNA) = 10. Hep-55.1C tumor-bearing mice: n (untreated) = 4; n (OH-RNA) = 4; n (ppp-RNA) = 5).

Results

Table 1: Statistic outcome of survival analysis of RIL-175 and Hep-55.1C tumor-bearing mice after ppp-RNA therapy. Listed p-values were calculated via log-rank test of survival analysis depicted in Figure 9.

Cell line	Parameter	p-value
RIL-175	untreated vs. OH-RNA	0.7102
	untreated vs. ppp-RNA	< 0.0001
	OH-RNA vs. ppp-RNA	< 0.0001
Hep-55.1C	untreated vs. OH-RNA	0.0725
	untreated vs. ppp-RNA	0.0318
	OH-RNA vs. ppp-RNA	0.7063

5.4.2 Immune monitoring during ppp-RNA therapy

It could be demonstrated that systemic ppp-RNA treatment positively impacts the survival of mice bearing liver tumors (Figure 9, Table 1). The immunological effects induced by this therapy, such as cytokine induction and immune cell activation, were further examined.

5.4.2.1 Orthotopic Hep-55.1C model

Hep-55.1C tumors were orthotopically induced in the left liver lobe of C57BL/6 mice. Mice were treated with repeated injections of ppp-RNA intravenously. The systemic application of ppp-RNA significantly increased plasma levels of the pro-inflammatory chemokine IP-10 (Figure 10). OH-RNA also induced IP-10 production, albeit lower levels, pointing to a TLR-mediated off-target effect of the RNA (Ellermeier *et al.*, 2013). The systemic ppp-RNA treatment led to the influx of CD8$^+$ T cells in the tumor tissue and to a slight reduction of splenic NK cells. Changes in the numbers of CD4$^+$ T cells were not statistically significant (Figure 11). Furthermore, NK cells in the tumor and spleen showed increased expression levels of the activation marker CD69 (Figure 12).
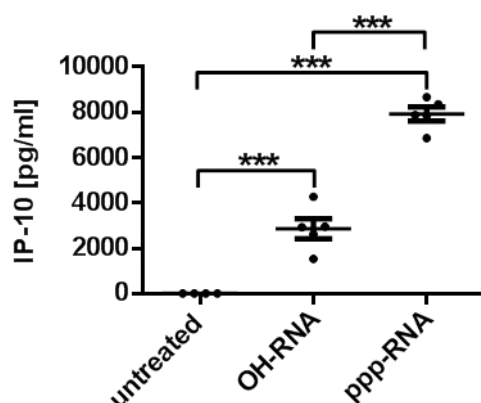
Figure 10: Systemic ppp-RNA therapy increases IP-10 plasma levels in tumor-bearing mice. Hep-55.1C tumors were induced orthotopically in the left liver lobe of C57BL/6 mice. Mice were treated with 50 µg ppp-RNA complexed to in vivo-jetPEI® or control RNA (OH-RNA) on day 5 after tumor inoculation via i.v. injection. Untreated mice served as control. Blood was drawn 4 h after ppp-RNA administration and IP-10 plasma levels were determined via ELISA. Results are shown as mean and error bars represent SEM. Statistical analysis was performed via ordinary one-way ANOVA and Tukey´s multiple comparisons tests (n = 4; 5; 5 for untreated; OH-RNA; ppp-RNA, respectively). Asterisks indicate p-value: *** < 0.001.

[A] Tumor

CD8⁺ T cells **CD4⁺ T cells** **NK cells**

[B] Spleen

CD8⁺ T cells **CD4⁺ T cells** **NK cells**
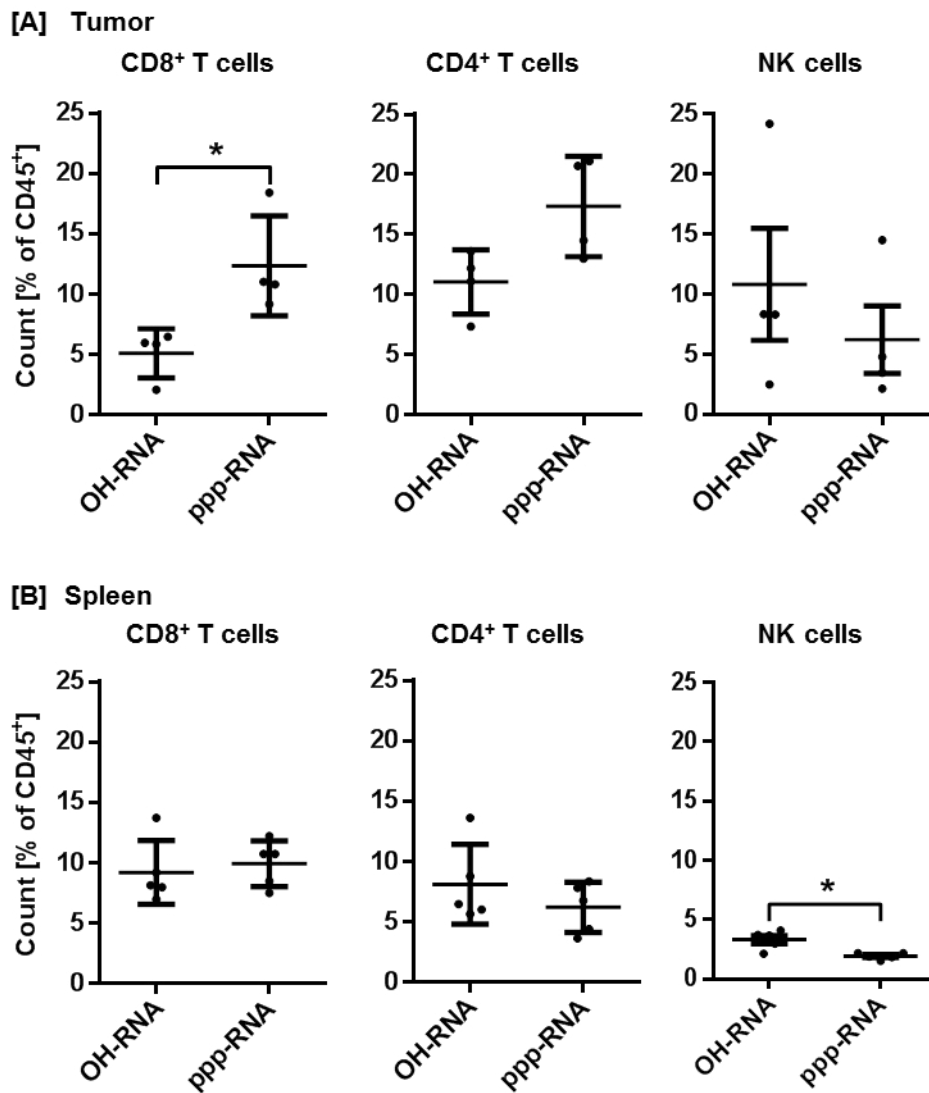
Figure 11: Accumulation of T cells at the tumor site after systemic ppp-RNA immunotherapy. Hep-55.1C tumors were induced orthotopically in the left liver lobe of C57BL/6 mice. Mice were treated with 50 µg ppp-RNA complexed to in vivo-jetPEI® or control RNA (OH-RNA) on days 5, 9, 12, 16, 19 and 23 after tumor induction via i.v. injection. 12 h after the last ppp-RNA injection mice were sacrificed and spleens and tumors were explanted. Immune cell populations were analyzed via flow cytometry. CD4⁺ T cells were defined as CD45⁺CD3⁺CD4⁺, CD8⁺ T cells as CD45⁺CD3⁺CD4⁺, NK cells as CD45⁺CD3⁻NK-1.1⁺. Results are shown as mean and error bars represent SEM. Statistical analysis was performed using an unpaired t test with Welch's correction (tumor: n = 4; spleen: n = 5). Asterisk indicates p-value: * < 0.05.
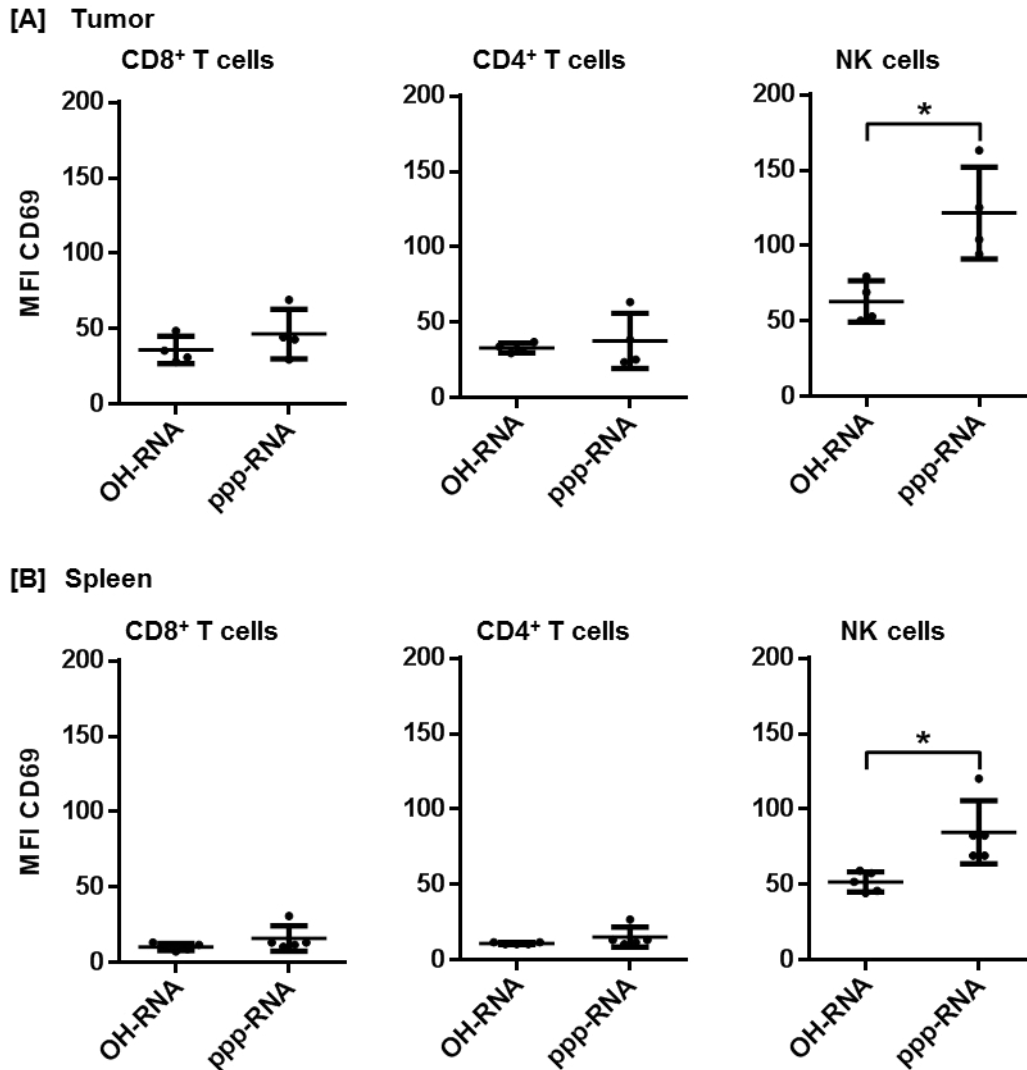
[A] Tumor

[B] Spleen

Figure 12: Systemic ppp-RNA application leads to the activation of NK cells in tumor and spleen. Hep-55.1C tumors were induced orthotopically in the left liver lobe of C57BL/6 mice. Mice were treated with 50 µg ppp-RNA complexed to in vivo-jetPEI® or control RNA (OH-RNA) on days 5, 9, 12, 16, 19 and 23 after tumor induction via i.v. injection. 12 h after the last ppp-RNA injection mice were sacrificed and spleens and tumors were explanted. Expression of CD69 of immune cells was analyzed via flow cytometry. CD4$^+$ T cells were defined as CD45$^+$CD3$^+$CD4$^+$, CD8$^+$ T cells as CD45$^+$CD3$^+$CD4$^+$, NK cells as CD45$^+$CD3$^-$NK-1.1$^+$. Results are shown as mean and error bars represent SEM. Results are shown as mean and error bars represent SEM. Statistical analysis was performed using an unpaired t test with Welch's correction (tumor: n = 4; spleen: n = 5). Asterisk indicates p-value: * < 0.05.

5.4.2.2   Orthotopic RIL-175 model

RIL-175 liver tumors were orthotopically induced in C57BL/6 mice and mice were systemically treated with repeated injections of ppp-RNA. The systemic ppp-RNA therapy did not lead to a significant increase of T cells and NK cells at the tumor site or in the spleen. However, CD8$^+$ T cells were slightly increased at the tumor site after treatment with therapeutic RNA in comparison to control groups, however, the difference lacked statistical significance (Figure 13). Despite strong cytokine induction (Figure 20), only activation of NK cells, but not of CD4$^+$ and CD8$^+$ T cells, could be observed at the tumor site in

comparison to the control group upon ppp-RNA therapy, as assessed by upregulation of the early activation marker CD69 and FasL (Figure 14). Furthermore, RIG-I-based therapy induced activation of CD8$^+$ T cells, NK cells and CD4$^+$ T cells in the spleen (Figure 15).
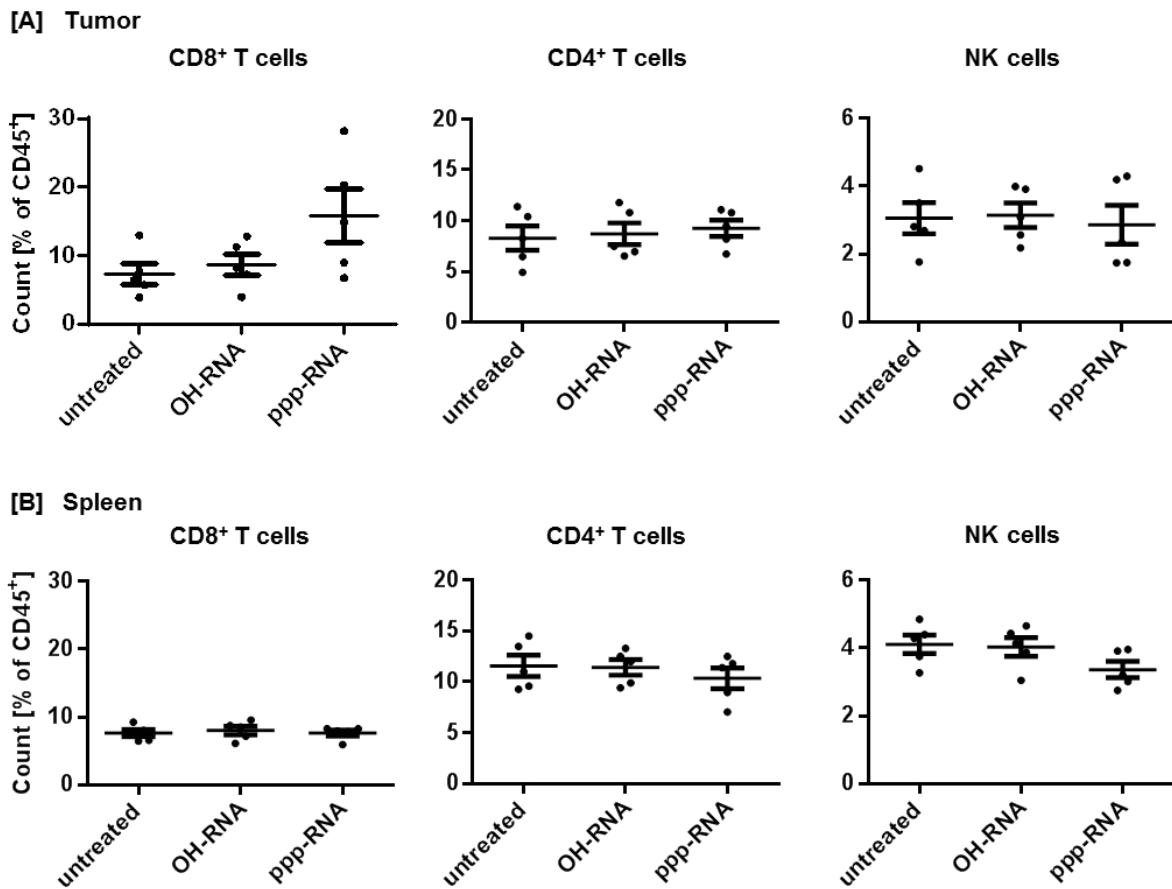
Figure 13: Quantitative analysis of immune cell populations in tumor tissue and spleen after systemic ppp-RNA immunotherapy. RIL-175 tumors were induced orthotopically in the left liver lobe of C57BL/6 mice. Mice were treated with 50 µg ppp-RNA complexed to in vivo-jetPEI® or control RNA (OH-RNA) on days 10 and 14 after tumor induction via i.v. injection. Untreated mice served as control. 12 h after the last ppp-RNA injection mice were sacrificed and tumors were explanted. Expression of CD69 and FasL by immune cells was analyzed via flow cytometry. CD4$^+$ T cells were defined as CD45$^+$CD3$^+$CD4$^+$, CD8$^+$ T cells as CD45$^+$CD3$^+$CD4$^+$, NK cells as CD45$^+$CD3$^-$NK-1.1$^+$. Results are shown as mean and error bars represent SEM. Statistical analysis was performed via ordinary one-way ANOVA and Tukey´s multiple comparisons tests (n = 5 mice per group).

Results

[A] CD8⁺ T cells
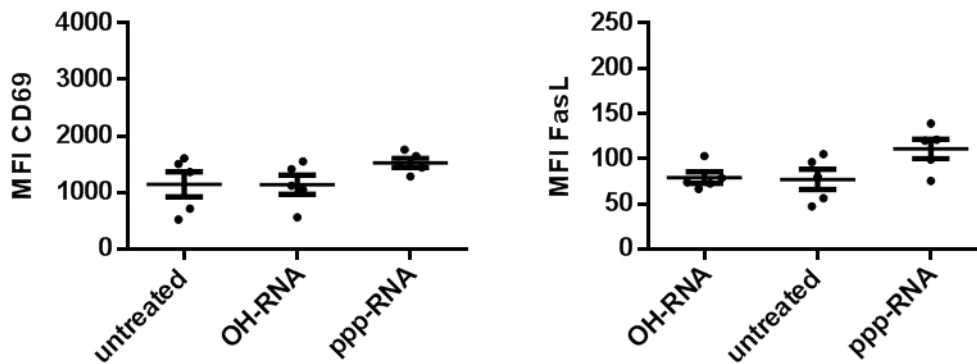
[B] CD4⁺ T cells
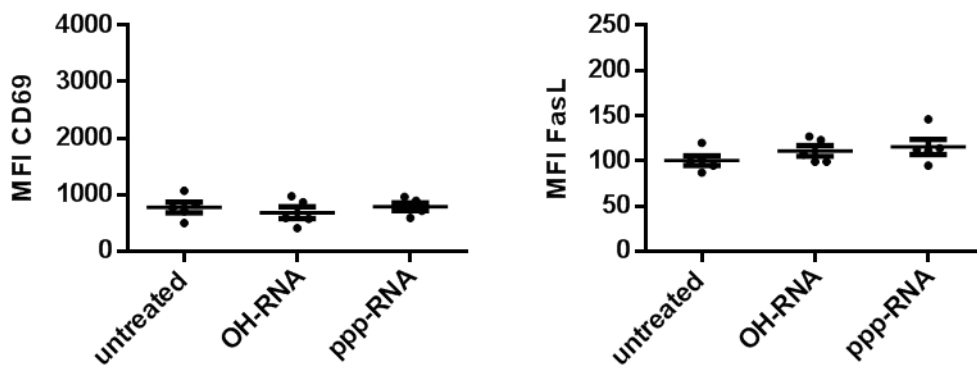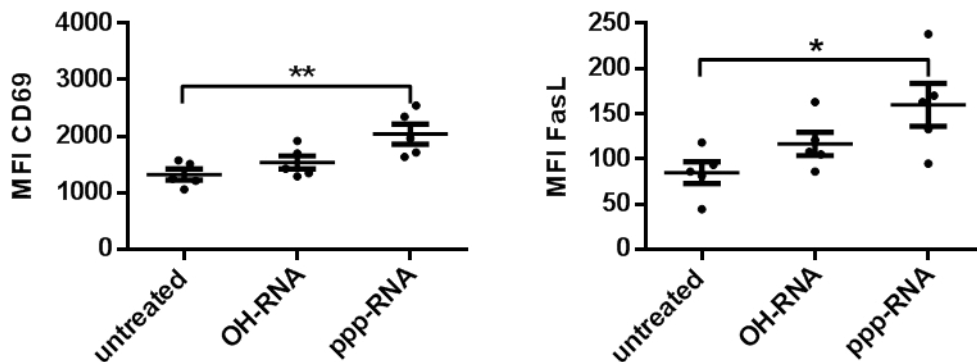
[C] NK cells

Figure 14: Systemic ppp-RNA application leads to the activation of NK cells at the tumor site. RIL-175 tumors were induced orthotopically in the left liver lobe of C57BL/6 mice. Mice were treated with 50 µg ppp-RNA complexed to in vivo-jetPEI® or control RNA (OH-RNA) on days 10 and 14 after tumor induction via i.v. injection. Untreated mice served as control. 12 h after the last ppp-RNA injection mice were sacrificed and tumors were explanted. Expression of CD69 and FasL by immune cells was analyzed via flow cytometry. CD4⁺ T cells were defined as CD45⁺CD3⁺CD4⁺, CD8⁺ T cells as CD45⁺CD3⁺CD4⁺, NK cells as CD45⁺CD3⁻NK-1.1⁺. Results are shown as mean and error bars represent SEM. Statistical analysis was performed via ordinary one-way ANOVA and Tukey´s multiple comparisons tests (n = 5 mice per group). Asterisks indicate p-values: * < 0.05; **< 0.01.

Results

[A] CD8⁺ T cells

[B] CD4⁺ T cells

[C] NK cells

Figure 15: ppp-RNA immunotherapy leads to the activation of splenic T cells and NK cells. RIL-175 tumors were induced orthotopically in the left liver lobe of C57BL/6 mice. Mice were treated with 50 μg ppp-RNA complexed to in vivo-jetPEI® or control RNA (OH-RNA) on days 10 and14 after tumor induction via i.v. injection. Untreated mice served as control. 12 h after the last ppp-RNA injection mice were sacrificed and spleens were explanted. Expression of CD69 and FasL by immune cells was analyzed via flow cytometry. CD4⁺ T cells were defined as CD45⁺ CD3⁺ CD4⁺, CD8⁺ T cells as CD45⁺ CD3⁺ CD4⁺, NK cells as CD45⁺ CD3⁻ NK-1.1⁺. Results are shown as mean and error bars represent SEM. Statistical analysis was performed via ordinary one-way ANOVA and Tukey´s multiple comparisons tests (n = 5 mice per group). Asterisks indicate p-values: * < 0.05; **< 0.01.

5.4.3   Toxicity of ppp-RNA therapy

To investigate potential toxic hematological side effects caused by the systemic ppp-RNA immunotherapy, the distribution of immune cell populations in the blood was examined. The relative frequency of T cells, NK cells, NKT cells and B cells in the blood was significantly reduced 24 h after RNA injection and recovered after 48 h, whereas NK cell levels appeared to be slightly elevated at this time point. Conversely, the levels of blood monocytes were significantly increased 24 h after injection of ppp-RNA and decreased after 48 h (Figure 16 A). To assess kidney or liver damage induced by the ppp-RNA immunotherapy, plasma levels of urea, GOT and GPT were analyzed. No significant differences between untreated mice and mice treated with control RNA or ppp-RNA could be observed regarding GOT and GPT levels (Figure 16 B).
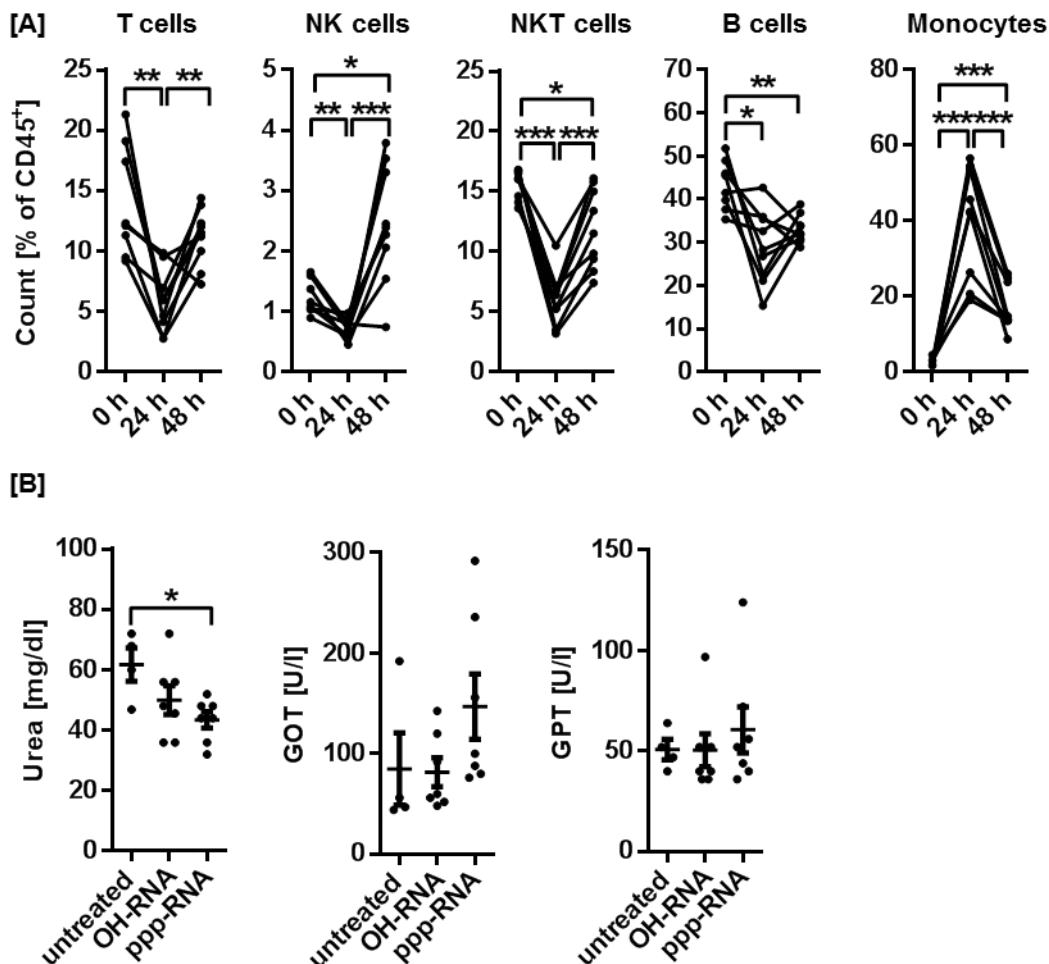
Figure 16: ppp-RNA immunotherapy does not cause long lasting severe adverse effects. [A] Frequency of T (CD45+CD3+), NK (CD45+CD3-NK-1.1+), NKT (CD45+CD3+NK-1.1+), B cells (CD45+CD19+) and monocytes (CD45+CD14+) were determined via flow cytometry 0 h, 24 h and 48 h after i.v. injection of 50 µg ppp-RNA complexed to in vivo-jetPEI® in healthy non-tumor bearing mice. Results are shown as mean and error bars represent SEM. Statistical analysis was performed using a paired t test (n = 8 for 0 h and n = 9 for 24 and 48 h, respectively). [B] Hepa1-6 tumors were induced orthotopically in the left liver lobe of C57BL/6 mice. Mice were treated with 50 µg ppp-RNA complexed to in vivo-jetPEI® or control RNA (OH-RNA) on days 5, 9, 12, 16, 19 and 23 after tumor induction via i.v. injection. Urea, GOT and GPT plasma values were determined 12 h after the last injection. Results are shown as mean and error bars represent SEM. Statistical analysis was performed via

Results

ordinary one-way ANOVA and Tukey´s multiple comparisons tests (n = 4 for untreated; n = 7 for OH-RNA and ppp-RNA, respectively). Asterisks indicate p-values: * < 0.05; ** < 0.01; *** < 0.001.

5.4.4 Immune-mediated effector mechanisms

In order to address the role of the immune system for the therapeutic efficacy of the ppp-RNA-based therapy, RIL-175 tumors were orthotopically induced in immune-deficient NOD-*scid IL2Rγ^{null}* (NSG) mice and treated with repeated injections of ppp-RNA intravenously starting on day 5 after tumor induction. Mice treated with the therapeutic RNA had no benefit concerning survival in comparison to the untreated group (Figure 17). Interestingly, mice succumbed much quicker to the tumor challenge than wild-type mice (see Figure 9).
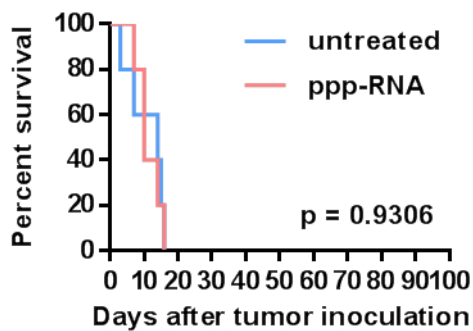
Figure 17: The immune system plays a critical role for the therapeutic efficacy of ppp-RNA-based therapy. RIL-175 tumors were orthotopically induced in the left liver lobe of NOD-*scid IL2Rγ^{null}* mice. Mice were treated with 50 µg ppp-RNA complexed to in vivo-jetPEI® or control RNA (OH-RNA) on days 5, 9 and 12 after tumor induction via i.v. injection. Survival was monitored and is depicted as Kaplan-Meier curve; p-values were calculated performing a log-rank test (n = 5 mice per group).

5.4.4.1 Influence of T and NK cells on therapeutic efficacy

To narrow down which immune cell population is involved in the therapeutic mode of action, CD4^+ T cells, CD8^+ T cells or NK cells were depleted via anti-CD4, anti-CD8 or anti-NK-1.1 antibody administration, respectively, in RIL-175 tumor-bearing mice prior to ppp-RNA injections. The depletion of these immune cell populations did not lead to significantly different IP-10 plasma levels in comparison to mice injected with the respective isotype (IgG) prior to ppp-RNA (Figure 18). Interestingly, the therapeutic effect was completely abolished after the depletion of CD8^+ T cells, whereas the depletion of NK cells had no impact on the therapeutic efficacy (Figure 18, Table 2). Depletion of and CD4^+ also decreased therapeutic efficacy, however statistical significance was not reached (p = 0.07).
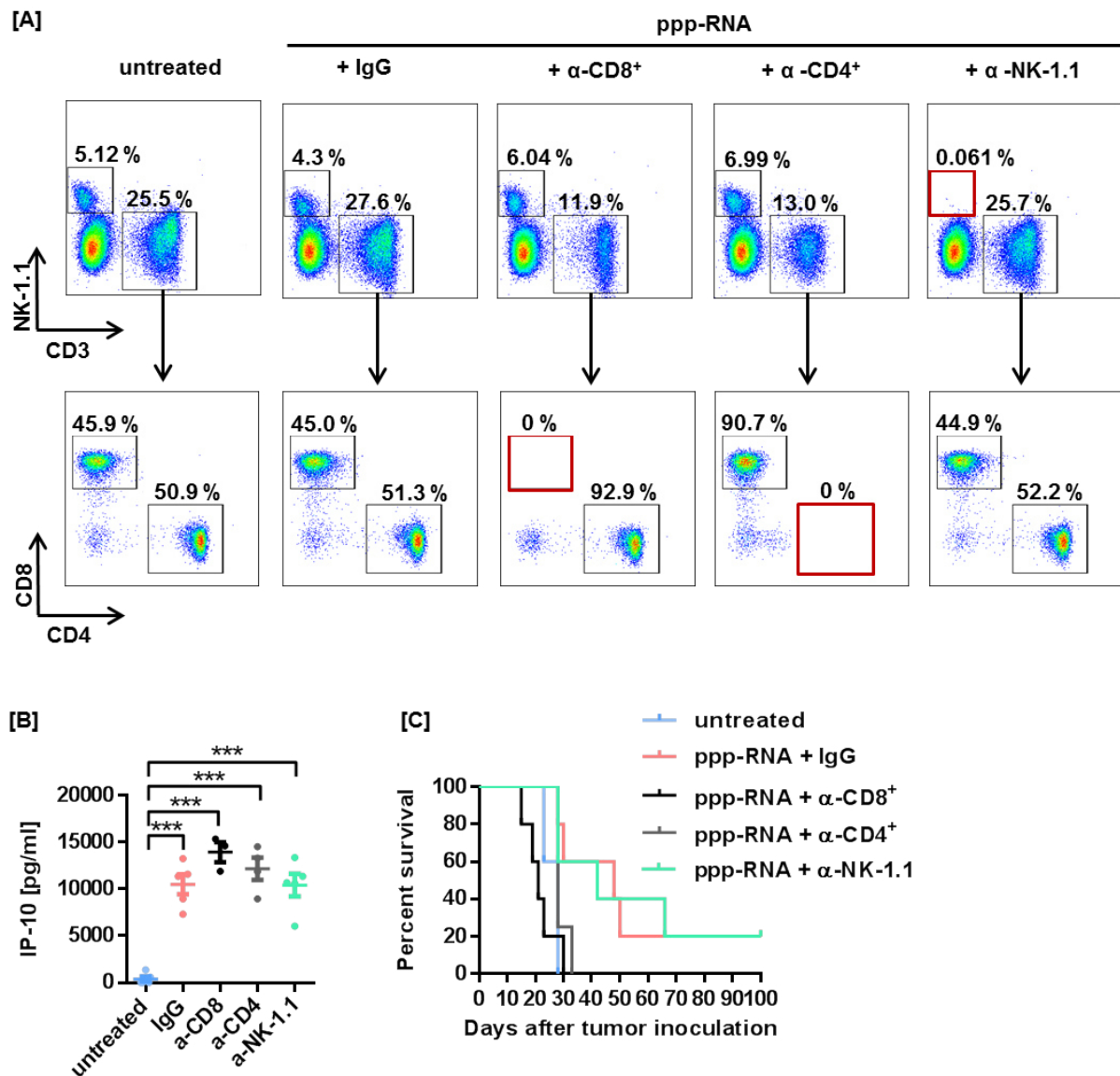
Figure 18: Therapeutic efficacy of ppp-RNA immunotherapy is CD8+ and CD4+ T cell dependent. RIL-175 tumors were orthotopically induced in the left liver lobe of C57BL/6 mice. Mice were treated with 50 µg ppp-RNA complexed to in vivo-jetPEI® or control RNA (OH-RNA) on days 5, 9, 12, 16, 19 and 23 after tumor inoculation via i.v. injection. α-CD8, α-CD4 and α-NK-1.1 depleting antibodies or respective isotype control (IgG) were administered in addition via i.p. injection 24 h prior to RNA injection. [A] Blood was drawn 24 h after injection of depleting antibodies and immune cell populations were analyzed via flow cytometry. Plots shown were gated on CD45+ cells. Depleted immune cell populations are highlighted in red. Depicted is one representative data set (n = 5 mice per group; n = 4 for ppp-RNA + α-CD4). [B] Blood was drawn 4 h after the fifth therapy and IP-10 plasma levels were determined via ELISA. Results are shown as mean and error bars represent SEM. Statistical analysis was performed via ordinary one-way ANOVA and Tukey´s multiple comparisons tests (n(untreated) = 5; n(ppp-RNA + IgG) = 5; n(ppp-RNA + α-CD8) = 3; n(ppp-RNA + α-CD4) = 4; n(ppp-RNA + α-NK) = 5). Asterisks indicate p-value: *** < 0.001. [C] Survival was monitored for up to 100 days and is depicted as Kaplan-Meier curve; p-values were calculated performing a log-rank test and are listed in Table 2 (n = 5 mice per group; n = 4 for ppp-RNA + α-CD4).

Table 2: Statistic outcome of survival analysis after depletion of CD8⁺, CD4⁺ and NK cells in RIL-175 tumor-bearing mice treated with ppp-RNA immunotherapy. Listed p-values were calculated via log-rank test of survival analysis depicted in Figure 18.

Table 2: Statistic outcome of survival analysis after depletion of CD8$^+$, CD4$^+$ and NK cells in RIL-175 tumor-bearing mice treated with ppp-RNA immunotherapy. Listed p-values were calculated via log-rank test of survival analysis depicted in Figure 18.

Parameter	p-value
ppp-RNA + IgG vs. untreated	0.0116
ppp-RNA + IgG vs. ppp-RNA + a-CD8	0.0136
ppp-RNA + IgG vs. ppp-RNA + a-CD4	0.0712
ppp-RNA + IgG vs. ppp-RNA + a-NK	0.9972

5.4.4.2 Analysis of treatment-induced immunological memory response

Mice that survived the tumor challenge due to ppp-RNA treatment longer than 100 days were rechallenged with the same tumor cells subcutaneously in order to investigate a potential formation of an immunological memory. All of the rechallenged mice rejected the tumor while naïve control mice all developed a tumor (Figure 19).
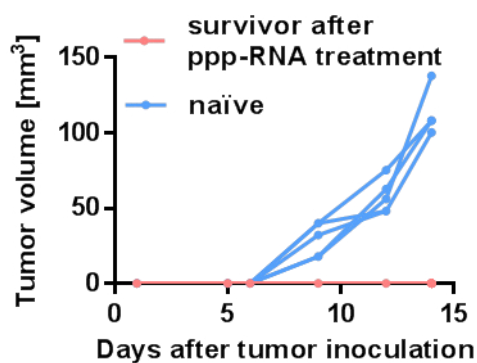
Figure 19: ppp-RNA immunotherapy mediates immunological memory. Surviving mice of prior experiments that had rejected their orthtotopic RIL-175 tumors upon ppp-RNA treatment (see Figure 18, Figure 20, Figure 22) were rechallenged with tumor cells s.c. after at least 100 days following the primary tumor challenge (n = 8). Naïve mice (n = 5) served as control. Tumor growth curves of individual mice are shown.

Results

5.4.4.3 Influence of systemic MAVS and type I IFN signaling on treatment response

To closer examine the signaling pathway triggering the therapeutic efficacy of the ppp-RNA-based immunotherapy, the influence of systemic RLH and type I IFN signaling was investigated *in vivo*. To this end, *Mavs$^{-/-}$* and *Ifnar1$^{-/-}$* mice on C57BL/6 background were orthotopically induced with RIL-175 tumors and treated with repeated i.v injections of ppp-RNA. Studies revealed a moderate decrease of IP-10 plasma levels after ppp-RNA treatment in MAVS- and a significant decrease in IFNAR1-deficient mice, compared to wild-type mice. Of note, compared to wild-type mice, survival was not different in MAVS- and IFNAR1-deficient mice, indicating that systemic MAVS and IFNAR signaling is dispensable for the treatment efficacy (Figure 20, Table 3 and Table 4).
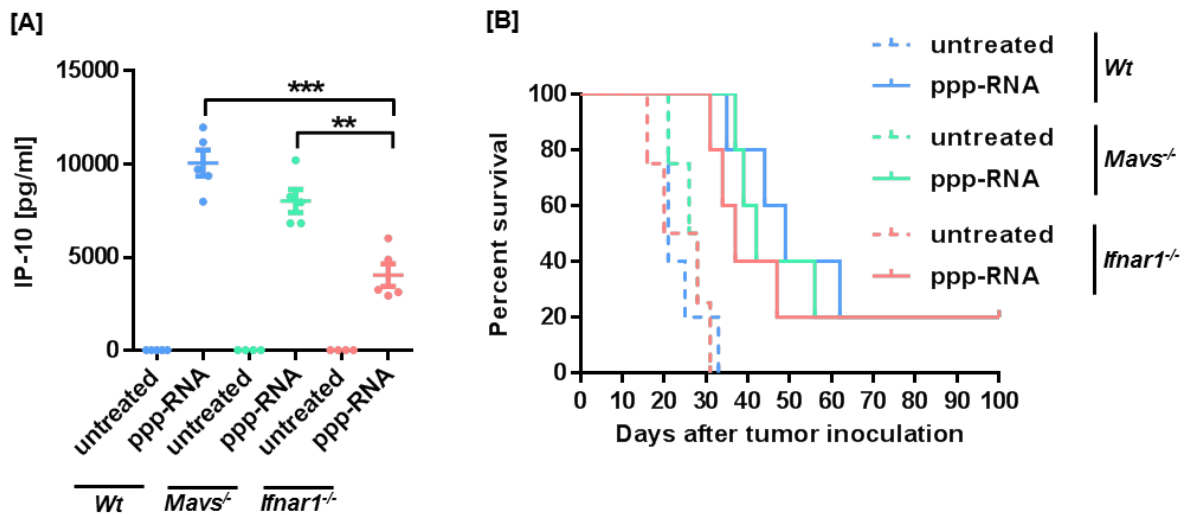
Figure 20: Therapeutic mode of action of ppp-RNA therapy is independent of systemic MAVS and IFNAR signaling. RIL175 tumors were orthotopically induced in the left liver lobe of C57BL/6 (*Wt*), *Mavs$^{-/-}$* and *Ifnar1$^{-/-}$* mice. Hosts were either treated with 50 µg ppp-RNA complexed to in vivo-jetPEI® on days 5, 9, 12, 16, 19 and 23 after tumor inoculation via i.v. injection or left untreated. [A] 4 h after the first therapy blood was drawn and IP-10 plasma levels were analyzed via ELISA. Results are shown as mean and error bars represent SEM. Statistical analysis was performed via ordinary one-way ANOVA and Tukey´s multiple comparisons tests; n = 4-5 mice per group. Asterisks indicate p-values: ** < 0.01; *** < 0.001. [B] Survival was monitored over 100 days and is depicted as Kaplan-Meier curve. P-values were calculated performing a log-rank test and are listed in Table 3. Median survival was calculated and is listed in Table 4 (n = 4-5 mice per group).

Table 3: Statistic outcome of survival analysis of RIL-175 tumor-bearing C57BL/6 mice with *Mavs*^{-/-} or *Ifnar1*^{-/-} background treated with ppp-RNA immunotherapy. Listed p-values were calculated via log-rank test of survival analysis depicted in Figure 20.

Genotype	Parameter	p-value
Wt	untreated vs. ppp-RNA	0.0015
Mavs^{-/-}	untreated vs. ppp-RNA	0.0027
Ifnar1^{-/-}	untreated vs. ppp-RNA	0.0072
Wt vs. Mavs^{-/-}	ppp-RNA vs. ppp-RNA	0.7462
Wt vs. Ifnar1^{-/-}	ppp-RNA vs. ppp-RNA	0.4914
Mavs^{-/-} *vs. Ifnar1*^{-/-}	ppp-RNA vs. ppp-RNA	0.5852

Table 4: Median survival of RIL-175 tumor-bearing C57BL/6 mice with *Mavs*^{-/-} or *Ifnar1*^{-/-} background treated with ppp-RNA immunotherapy. Listed median survival was calculated from survival analysis depicted in Figure 20.

Genotype	Treatment	Median survival [d]
Wt	untreated	21
	ppp-RNA	49
Mavs^{-/-}	untreated	27
	ppp-RNA	42
Ifnar1^{-/-}	untreated	24
	ppp-RNA	37

5.4.4.4 Combination of ppp-RNA therapy with checkpoint inhibition

In the previous experiments it was shown that T cells are crucially involved in the mode of action of the RIG-I based immunotherapy. As PD-L1 is an IFN-stimulated gene and therefore likely upregulated after ppp-RNA stimulation, blocking of the PD-1/PD-L1 axis may result in a stronger anti-tumoral T cell response. Murine (RIL-175, Hep-55.1C, Hepa1-6) and human (Huh7, Hep3B) HCC cells were analyzed for their expression of PD-L1 after transfection with ppp-RNA. The analysis showed that PD-L1 expression is significantly increased in all the investigated tumor cell lines after ppp-RNA stimulation (Figure 21).

In order to try to improve therapy´s efficacy, ppp-RNA was combined with repeated injections of an α-PD-1 blocking antibody. The analysis revealed that mice strongly benefited from the combination of ppp-RNA and checkpoint inhibition in comparison to ppp-RNA-treatment alone in the RIL-175 model with 60 % of mice showing complete tumor control up to 100 days, but not in the Hep-55.1C model (Figure 22, Table 5 and Table 6).
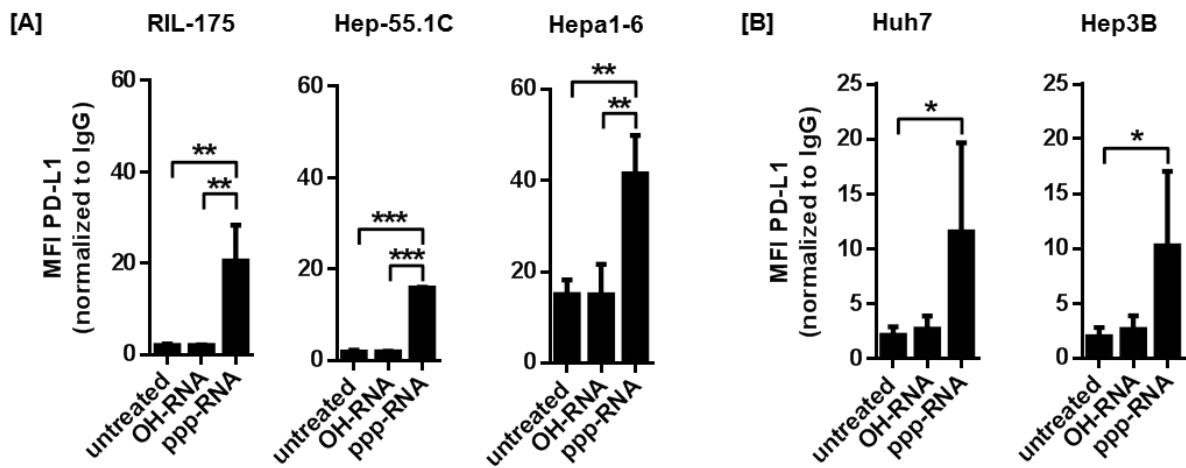
Figure 21: Stimulation of tumor cells with ppp-RNA induces PD-L1 expression. [A] Murine and [B] human HCC cells were transfected with 40 nM ppp-RNA, 40 nM control RNA (OH-RNA) or left untreated. PD-L1 expression was analyzed 48 h later via flow cytometry. Results are shown as mean of three (murine) and four (human) experiments, respectively. Error bars represent standard deviation. Statistical analysis was performed via ordinary one-way ANOVA and Tukey´s multiple comparisons tests. Asterisks indicate p-values: * < 0.05; ** < 0.01; *** < 0.001.
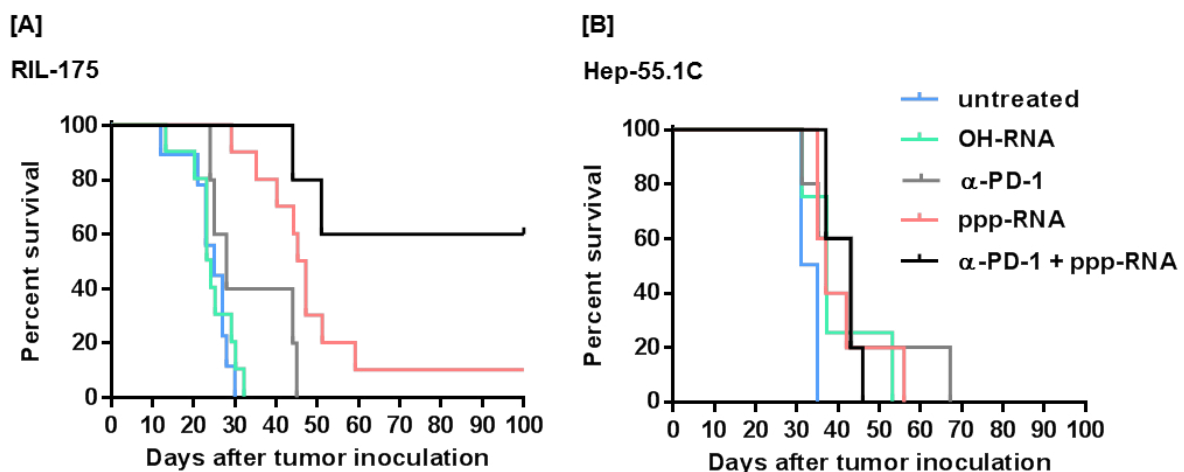
Figure 22: Combination of ppp-RNA therapy with checkpoint inhibition increases median survival of RIL-175 tumor-bearing mice. [A] RIL-175 or [B] Hep-55.1C tumors were induced orthotopically in the left liver lobe of C57BL/6 mice. Mice were treated with 50 µg ppp-RNA complexed to in vivo-jetPEI® or control RNA (OH-RNA) on days 5, 9, 12, 16, 19 and 23 after tumor inoculation via i.v. injection. 100 µg blocking α-PD-1 antibody were administered i.p. on days 4, 11 and 18. Survival was monitored over 100 days and is depicted as Kaplan-Meier curve; p-values were calculated performing a log-rank test and are listed in Table 5. Median survival of RIL-175 tumor-bearing mice was calculated and is listed in Table 6 (RIL-175 tumor-bearing mice: n(untreated) = 9; n(OH-RNA) = 10; n(ppp-RNA) = 10; n (α-PD-1) = 5; n(α-PD-1 + ppp-RNA) = 5. Hep-55.1C tumor-bearing mice: n(untreated) = 4; n(OH-RNA) = 4; n(ppp-RNA) = 5; n (α-PD-1) = 5; n(α-PD-1 + ppp-RNA) = 5).

Results

Table 5: Statistic outcome of RIL-175 and Hep-55.1C tumor-bearing C57BL/6 mice treated with ppp-RNA in combination with checkpoint inhibition. Listed p-values were calculated via log-rank test of survival analysis depicted in Figure 22.

Cell line	Parameter	p-value
RIL-175	untreated vs. OH-RNA	0.7102
	untreated vs. ppp-RNA	< 0.0001
	untreated vs. α-PD-1	0.0943
	OH-RNA vs. ppp-RNA	< 0.0001
	ppp-RNA vs. α-PD-1 + ppp-RNA	0.0604
Hep-55.1C	untreated vs. OH-RNA	0.0725
	untreated vs. ppp-RNA	0.0318
	untreated vs. α-PD-1	0.0882
	OH-RNA vs. ppp-RNA	0.7063
	ppp-RNA vs. α-PD-1 + ppp-RNA	0.7146

Table 6: Median survival of RIL-175 tumor-bearing C57BL/6 mice treated with ppp-RNA in combination with checkpoint inhibition. Listed median survival was calculated from survival analysis depicted in Figure 22.

Treatment	Median survival [d]
untreated	25
OH-RNA	24
ppp-RNA	46
α-PD-1	28
ppp-RNA + α-PD-1	undefined

6   Discussion

Hepatocellular carcinoma (HCC) ranks amongst the most aggressive cancer types with an overall 5-year survival rate of only 17 % (Siegel *et al.*, 2015). In most cases, HCC is diagnosed at late stage and surgical excision or local ablative destruction of the tumor is not possible. In some cases, liver transplantation is another treatment option. However, the growing number of potential recipients is much higher than the number of available organs (reviewed in Slotta *et al.*, 2015). The development of new drugs, acting at the molecular level, has improved treatment options of HCC. The discovery of targeted therapies, by blocking specific receptors, such as VEGFR (vascular endothelial growth factor receptors) and c-Met, and their downstream signaling, prevent or at least delay tumor growth with benefits regarding survival time (reviewed in Li and Wang, 2016; Zhang and Finn, 2016). Also, in the field of immunotherapy, there are therapeutic strategies that have already made it into clinical trials. While these new approaches, for example based on cancer vaccines and checkpoint inhibitors, may look promising, they still need to be fully explored (reviewed in Buonaguro *et al.*, 2013; Greten *et al.*, 2015; Hong *et al.*, 2015). However, there is a strong medical need for developing new therapeutic interventions. The scientific study of an immunotherapy targeting receptors of the innate immune system is subject of this work. It is based on years of exploration of the cytosolic helicase RIG-I as target for cancer immunotherapy and recent findings of research linked with RIG-I expression in HCC.

6.1   RIG-I signaling in murine and human HCC cell lines

The ubiquitously expressed cytosolic helicase RIG-I belongs to the family of RLH, which play a key role in the first line of defense against pathogenic RNA viruses. Its activation triggers the innate and the adaptive immune system by inducing a type I IFN response and the release of several pro-inflammatory cytokines (reviewed in Iwasaki and Medzhitov, 2010; Takeuchi and Akira, 2008). In addition, different working groups demonstrated that the activation of RLH, imitating a viral infection, via *in vitro*-transcribed or synthetic double stranded RNA induces the intrinsic mitochondrial and the extrinsic CD95-mediated apoptotic pathway, respectively (Besch *et al.*, 2009; Duewell *et al.*, 2014). This immunogenic form of apoptosis leads to enhanced antigen presentation by dendritic cells and activation of tumor-directed T cells (Duewell *et al.*, 2014). RIG-I has already been investigated as potential target in cancer research, including melanoma, pancreatic cancer, lung cancer, breast cancer and HCC (Duewell *et al.*, 2014; Ellermeier *et al.*, 2013; Funk, 2018; Lazić, 2017; Poeck *et al.*, 2008). Due to the autocrine signaling, which is caused upon RIG-I activation, agonists of RIG-I would provide one possible treatment option in the setting of cancer therapy (Kang *et al.*, 2004). In addition, the technical possibility to convert 5´-ppp-RNA into 5´-ppp-siRNA gives promising results to combine RIG-I activation and the silencing of specific oncogenes via RNAi within one molecule (Ellermeier *et al.*, 2013; Poeck *et al.*, 2008).

In order to address the idea of a RIG-I-based immunotherapy in HCC, the expression of the cytosolic helicase and its functionality was first assessed in human and murine HCC cell lines (sections 5.1 and 5.2). To this end 239 tissue micro arrays (TMA) of human HCC samples were tested positive for the expression of RIG-I, whereby the expression levels were categorized into three different levels: low, moderate and high (Figure 3). Further *in vitro* experiments confirmed that RIG-I signaling is functional in murine (Hep-55.1C, RIL-175, Hepa1-6) and human (Huh7, Hep3B) HCC cell lines, as stimulation with IFN-α and ppp-RNA increased the expression of RIG-I on mRNA and protein level (Figure 5). The transfection of the different cell lines led to the induction of IFN-β and subsequent upregulation of IFN-stimulated genes like MHC-I/HLA, RIG-I itself and IP-10 (Figure 5, Figure 6 and Figure 7). Thus, RIG-I signaling leads to its own amplification in a type I IFN-dependent positive feedback loop (Kang *et al.*, 2004; Schmidt *et al.*, 2009). However, there was no MHC-I expression detected on the surface of Hepa-1-6 cells, neither with nor without transfection of ppp-RNA (Figure 6). As the cell line was originally generated from the C57L-mouse strain, and not from C57BL/6-mice (origin of RIL-175 and Hep-55.1C cells) the haplotype of this cell line (H-2k^{bc}) differs from the one with C57BL/6-background (H-2k^{b}) (BioLegend). This may be the reason why there was no expression of MHC-I detected with commercially available mAb. Another reason may be that the cell line is impaired in MHC-I expression or signaling, respectively. The reduction of the cell viability after stimulation of the HCC cells with ppp-RNA results from the induction of the intrinsic apoptotic pathway (Figure 6 and Figure 7). These findings are in line with Besch *et al.* (2009), who first showed that endogenous apoptosis cannot only be triggered by RIG-I signaling via the induction of type I IFN, but also be initiated IFN-independently upon ppp-RNA stimulation of tumor cells. Together, these findings indicate that RIG-I is expressed and functional in HCC, which is in line with previous work in our lab and sets the basis for *in vivo* therapy studies for the development of ppp-RNA-based immune therapeutics (Funk, 2018; Lazić, 2017).

6.2   Establishment of suitable HCC mouse models

After having demonstrated that the RIG-I signaling pathway is functional in murine and human HCC cell lines *in vitro* (sections 5.1 and 5.2) the efficacy of the ppp-RNA-based immunotherapy was to be further tested *in vivo*. To this end, the model of choice was the orthotopic transplantation of murine HCC cells in the left liver lobe of syngeneic C57BL/6 mice (section 5.3). Implantation models are frequently used for the pre-clinical investigation of new drugs with the advantage of creating a closer setting to human cancer regarding the tumor microenvironment and morphology of the tumor than in subcutaneous models (reviewed in Bibby, 2004; Khanna and Hunter, 2005; Leenders *et al.*, 2008). In addition, using immune competent mice provides an intact immune system serving as a proof of concept for a therapy´s efficacy and mode of action. It has also been described as a model

being suitable for testing immune checkpoint inhibitors in an experimental *in vivo*-setting, as tumor cells and immune cells can fully interact with each other. However, tumor development is neither based on chronic inflammation due to rapid tumor growth nor on mutational load (reviewed in Sanmamed *et al.*, 2016), making syngeneic models less suitable for therapies acting on the onset of tumor development and for drugs targeting specific mutations.

The orthotopic transplantation of Hep55-1.C and RIL-175 cells led to steady tumor cell growth and resulted in tumor-related death of mice. The establishment of a Hepa1-6 HCC *in vivo* model was not successful, as only 3 out of 7 transplanted mice developed a liver tumor (Figure 8). One reason therefore may be the discrepancies of the haplotype between the transplanted cells (Hepa1-6: C57L-mouse strain) and the host (C57BL/6 mouse strain). In a strict sense, the Hepa1-6 model is not syngeneic with the C57BL/6 mouse strain. Thus, scientific publications using this murine HCC model should be interpreted with caution.

6.3 Therapeutic efficacy and immune stimulatory potential of the RIG-I-based immunotherapy

HCC is characterized by a pronounced immunosuppression due to high levels of immunosuppressive cytokines, such as TGF-β and IL-10, impaired antigen presentation and accumulation of regulatory T cells and myeloid derived suppressor cells (reviewed in Hato *et al.*, 2014; Makarova-Rusher *et al.*, 2015). Recent studies implicate lymphocyte infiltration as prognostically favorable pointing out a role for CD8^{+} T cells in tumor control (Fatourou and Koskinas, 2009; Ikeguchi *et al.*, 2004; Vesely *et al.*, 2011). For an efficient immunotherapy it is therefore important to overcome tumor-promoting immunosuppression by targeted activation of immune cells. In order to investigate RIG-I as potential target for HCC immunotherapy *in vivo*, the efficacy of the therapeutic RNA and its immune stimulatory potential were investigated using the RIL-175 and Hep-55.1C HCC mouse models (sections 5.4.1. and 5.4.2). The systemic ppp-RNA therapy of RIL-175 tumor-bearing mice significantly prolonged survival in comparison to the respective control groups. In contrast, mice with Hep-55.1C tumors did not benefit from the RIG-I-based immunotherapy (Figure 9, Table 1). Similar findings as in the RIL-175 *in vivo* model have been reported for models of melanoma and pancreatic carcinoma. Poeck *et al.* (2008) could show, that treatment of mice with subcutaneous B16-tumors significantly decelerated tumor growth. In addition, systemic treatment with ppp-RNA of mice with orthotopic Panc-02 tumors significantly prolonged survival of tumor-bearing mice (Ellermeier *et al.*, 2013).

The immunological effects induced by the ppp-RNA-based immunotherapy were further examined, also focusing on the difference between both *in vivo* models. The systemic injection of the therapeutic RNA significantly increased IP-10 plasma levels (Figure 10 and Figure 20) indicating an intact RIG-I signaling pathway (Schmidt *et al.*, 2009). In addition,

ppp-RNA therapy led to a significant accumulation of CD8$^+$ T cells at the tumor site. In this regard a positive trend could also be observed for CD4$^+$ T cells (Figure 11). Furthermore, the ppp-RNA´s potential to induce an immune response by assessing the upregulation of the early activation marker CD69 and FasL, the ligand of the death receptor CD95 (Fas), on T cells and NK cells could be demonstrated. FasL is expressed on the surface of T cells after its activation and triggers the extrinsic apoptosis upon binding to CD95 on target cells (reviewed in O'connell *et al.*, 1996). As CD95 is upregulated by tumor cells upon ppp-RNA treatment and its ligand, FasL, is upregulated on T and NK cells, FasL-mediated killing is likely an effector mechanism induced by this therapy. Activated NK cells were observed in the spleen and in the tumor of Hep-55.1C tumor-bearing mice (Figure 12). In the RIL-175 HCC model, activated CD8$^+$ T cells, CD4$^+$ T cells (in respect to CD69 upregulation) and NK cells in the spleen, as well as activated NK cells at the tumor site could be detected after ppp-RNA immunotherapy (Figure 14 and Figure 15). These results clearly point towards an immune mediated tumor control, which was clearly demonstrated in immune-compromised NOD-*scid IL2Rγ^{null}* mice (Figure 17).

The mode of action of the ppp-RNA immunotherapy was further studied evaluating the role of individual immune cell populations (section 5.4.4). The anti-tumor efficacy was CD4$^+$ and CD8$^+$ T cell-dependent, whereas NK cells were dispensable for the therapeutic effect (Figure 17 and Figure 18). In comparison, Poeck *et al.* (2008) found that the efficacy of ppp-RNA therapy is solely NK- and not CD8$^+$ T cell-dependent in a B16-based melanoma mouse model. It was further shown that treatment with ppp-RNA induces a protective immunological memory linking innate and adaptive immunity, as shown by complete tumor rejection in rechallenge experiments (Figure 19). The distinct role of T cells regarding the mechanism of action could be further investigated in a setting using adoptive T cell transfer in future experiments. Thereby CD4$^+$ and CD8$^+$ T cells of tumor-bearing mice, which were treated with ppp-RNA, could be transferred into naïve mice before tumor transplantation. By assessing the tumor growth in these mice it would be possible to gain further insights into the temporal dynamics and the interplay of these two cell types.The molecular mechanism of action was further demonstrated to be independent of systemic MAVS and IFNAR signaling using respective knockout (KO) mice, hinting towards a tumor cell-intrinsic RIG-I signaling response (Figure 20, Table 3). The median survival of *Ifnar1$^{-/-}$* mice, and also of *Mavs$^{-/-}$* mice, was not significantly reduced after ppp-RNA therapy in comparison to treated wild-type mice (Table 4). As endogenous IFN-α is essential for tumor surveillance and it has been already reported that mice with systemic *Ifnar1* KO are more susceptible for tumor growth, a decreased median survival of untreated *Ifnar1$^{-/-}$* mice in comparison to *Wt* mice would have been expected (Picaud *et al.*, 2002). Maybe the initial tumor load was too high and differences between the two mouse strains could not be observed. Particularly surprising

were the results regarding the *Ifnar1*^{-/-} mice, as APC, besides NK cells, need type I IFN for proper cross-priming of $CD8^+$ T cells (Diamond *et al.*, 2011; Fuertes *et al.*, 2011; Fuertes *et al.*, 2013). As $CD8^+$ T cells seemed to be vitally important for the therapy´s effectiveness (section 5.4.4.1), the $CD8^+$ T cell depletion experiments should be repeated in mice lacking IFNAR1 to confirm these findings. However, a significant difference in regards to the decrease of IP-10 plasma levels could be observed after ppp-RNA therapy from *Mavs*^{-/-} to *Ifnar1*^{-/-} mice, indicating that the induction of IP-10 in the plasma mainly depends on systemic IFNAR and also to some extent on systemic MAVS signaling (Figure 20). In what way the anti-tumoral effect of ppp-RNA therapy is mediated by intra-tumoral RIG-I signaling could be further assessed in an *in vivo* setting using RIG-I⁻deficient tumor cells transplanted into the respective knockout and wild-type mice, respectively. To further rule out that the therapy´s effect is IFN-α-dependent, the experiments could be performed using *Ifnar1*^{-/-} tumor cells and *Ifnar1*^{-/-} mice, respectively. However, in mouse models of pancreatic carcinoma, our working group found that systemic IFN-α therapy alone has no anti-tumoral efficacy (Hölz, 2018).

In summary, the systemic treatment with the therapeutic ppp-RNA induced a profound immune response in both murine HCC tumor models, but the fundamental difference between the two models, which ultimately led to the different therapeutic results, could not be clarified in this work. Regarding the Hep-55.1C-based tumor model one may speculate about immune escape mechanisms such as an immunosuppressive microenvironment mediated by T_{reg} and tumor-associated macrophages and the expression of immunosuppressive molecules such as PD-L1, as well as a defect in antigen presentation (reviewed in Beatty and Gladney, 2015). The resistance to apoptosis may also be taken into account (reviewed in Igney and Krammer, 2002). The given results point towards an intra-tumoral RIG-I signaling response (section 5.4.4.3). One point here to consider is the vascularization grade of Hep-55.1C and RIL-175 tumors regarding the proper delivery of the injected ppp-RNA into the tumor. This might be crucial for the therapy´s effectiveness. Going further, nucleic acid complexed to *in vivo*-jetPEI® is described to highly accumulate in the liver 24 h after intravenous injection (PerkinElmer Inc., 2013). *In vivo*-jetPEI®-Gal conjugated with galactose, the ligand of the asialoglycoprotein receptor (ASGP-R), which is highly expressed on hepatocytes, could be chosen for further experiments to improve the RNA´s proper delivery. In the context of tumor-targeted RNA delivery, one might also consider ppp-RNA loaded to nanoparticles, which are coated with liver homing-receptors. This is a smart approach to ensure appropriate drug delivery and to reduce off-target effects (reviewed in Kanasty *et al.*, 2013; Reddy and Couvreur, 2011). Some approaches have already successfully made it into clinical trials showing promising results for advanced HCC and drug-resistant liver cancer (Gao *et al.*, 2015; Merle *et al.*, 2006).

6.4 Safety and tolerability of systemic ppp-RNA treatment

In addition to the efficacy, safety and tolerability of the therapy were also investigated (section 5.4.3). It could be shown that repeated systemic treatment with ppp-RNA does not cause irreversible adverse events *in vivo.* There were no laboratory abnormalities in the sera of treated mice pointing towards an induced liver or kidney damage (Figure 16 B). A transient change in the composition of cells in the white blood cell count was observed. A significant decrease of relative numbers of peripheral T cells, NKT cells, NK cells and B cells occurred 24 h after therapy, however, cell numbers recovered on the next day (Figure 16 A). An opposite effect in this setting was observed for monocytes (Figure 16 A). The latter may be due to the fact that only relative cell numbers were assessed. The effect of a transient leukopenia after ppp-RNA therapy was already reported by Ellermeier *et al.* (2013). The reason therefore is still unknown, but one may speculate that immune cells accumulate in secondary lymphoid organs after injection of the immune stimulatory RNA. In addition, leukopenia is a known side effect of therapy with IFN-α or IFN-β, which is produced in large amounts during ppp-RNA treatment (Dusheiko, 1997; Goodin *et al.*, 1995).

A central question in the clinical setting remains the formulation of the therapeutic RNA. For this study the ppp-RNA was complexed to *in vivo*-jetPEI®, a polymer-based reagent that is also used in clinical trials. Nucleic acids formulated with this reagent and injected intravenously are reported to accumulate, among other sites, in the liver 24 h after administration (PerkinElmer Inc., 2013). One important point here to consider is that RIG-I signaling entails the considerable risk of a cytokine storm (Kaneda, 2013; Loo and Gale Jr, 2011; Matsushima-Miyagi *et al.*, 2012). It remains to be discussed, whether an intra-tumoral injection would be safer and potentially more effective. In this line, the intra-lesional administration of a RNA oligonucleotide-based RIG-I agonist complexed to PEI is currently under investigation in a phase I/II study in patients with injectable liver tumors or liver metastases (ClinicalTrials.gov, 2018c).

6.5 Improving ppp-RNA-based immunotherapy

Checkpoint inhibitors, such as mAb directed against PD-1 and PD-L1, are drugs braking tumor immune escape mechanisms that have revolutionized immunotherapy of cancer. PD-1 is expressed by B cells, T cells and NK cells, whereas its ligand PD-L1 is expressed on various non-lymphoid tissue. Upon activation of T cells, the PD-1/PD-L1 axis acts as counter-part of co-stimulatory molecules ensuring the equilibrium of immune activation and immune inhibition. T cells expressing PD-1 are inhibited from a proper anti-tumor response upon binding to its ligand PD-L1, which is expressed by tumor cells and myeloid cells in the tumor microenvironment (reviewed in Sharpe, 2017). Due to the fact that the PD-1/PD-L1 axis plays a crucial role in the immunosuppressive microenvironment of HCC (section 1.2), PD-1

blocking antibodies have recently made it into clinical HCC trials as single and combination therapy showing promising results in some patients (ClinicalTrials.gov, 2018a, 2018b; Truong *et al.*, 2016). One rationale of this work was to examine the therapeutic potential of ppp-RNA immunotherapy in combination with checkpoint inhibition (5.4.4.4). In this context the impact of RIG-I signalling on the PD-1/PD-L1 axis was first assessed *in vitro*. Flow cytometric studies revealed that activation of RIG-I led to the expression of PD-L1 on tumor cells of murine and human HCC cell lines (Figure 21), providing a scientific rationale for combining ppp-RNA therapy with checkpoint inhibition. Combination therapy induced a synergistic therapeutic effect in RIL-175 tumor-bearing mice. Percent survival rates were highly prolonged in this *in vivo* model (Figure 22, Table 5 and Table 6). Interestingly, no significant effect was observed in the Hep-55.1C tumor model (Figure 22), although a strong induction of PD-L1 after ppp-RNA treatment was demonstrated for this cell line *in vitro* (Figure 21). Here again, the crucial difference between the two *in vivo* models in terms of the therapeutic efficacy could not be clarified. Possibly other immune checkpoints are dominantly inhibiting the infiltrating T cells in this tumor model.

7   Conclusion

This study provides evidence that RIG-I is a novel target for HCC therapy. 239 human HCC tissue samples were analyzed for RIG-I expression by immunohistochemistry with almost 100 % of the tumors staining positive. Moreover, functional RIG-I signaling was confirmed in different murine and human HCC cell lines stimulated with ppp-RNA *in vitro*, leading to type I IFN and IP-10 production, upregulation of MHC-I expression, as well as apoptotic cell death.

In vivo efficacy of ppp-RNA-based therapy was demonstrated in mice bearing orthotopic RIL-175 liver tumors, significantly prolonging survival. The systemic application of the ppp-RNA was well tolerated, with a transient leukopenia being the only observed side effect at the tested dose. The lack of therapeutic efficacy in NSG mice, which are devoid of an intact immune system, and in mice that were depleted of CD4$^+$ and CD8$^+$ T cells point towards a T cell-mediated mechanism of action. Moreover, a sustained T cell memory was observed in successfully treated mice that were rechallenged with tumor cells, indicative of an immunogenic form of tumor cell death with T cell priming and T cell memory induction. The proposed mode of action of ppp-RNA-based immunotherapy in HCC is depicted in Figure 23.

Interestingly, in this study therapeutic efficacy of ppp-RNA therapy was not affected in mice lacking MAVS, an adaptor molecule required for RIG-I signaling. This finding points towards a dominant role of tumor cell-intrinsic RIG-I signaling, as this pathway was still intact in tumor cells. Experiments with RIG-I-/MAVS-deficient tumor cells are currently performed in our group to further study the impact of tumor cell-intrinsic RIG-I signaling. Moreover, mice lacking the type I IFN receptor were still benefiting from ppp-RNA therapy, arguing that type I IFN is dispensable for treatment efficacy.

Type I IFN signaling is known to upregulate the PD-1/PD-L1 axis thereby limiting overactive immune activation and potential tissue damage. From this perspective, the combination of RIG-I-based immunotherapy with α-PD-1 checkpoint inhibition is a promising rationale to enhance anti-tumor immune responses. In fact, combination therapy led to improved tumor control with complete tumor regression in 60 % of mice. No increase of toxicity was observed. Thus, combining ppp-RNA-based immune therapeutics with α-PD-1 mAb may offer new treatment options for patients suffering from HCC and deserves further preclinical and clinical investigation.
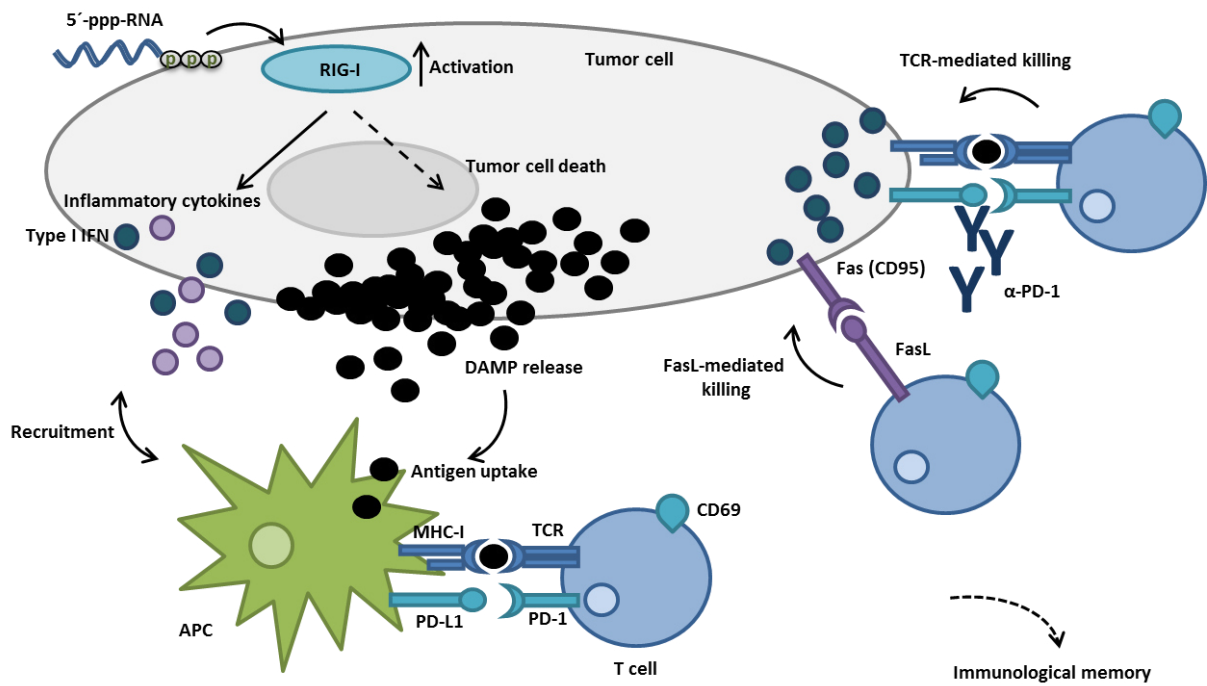
Figure 23: Proposed mode of action of ppp-RNA-based immunotherapy in HCC. Upon systemic ppp-RNA administration intra-tumoral RIG-I gets activated leading to the secretion of inflammatory cytokines and type I IFN as well as tumor cell death followed by DAMP (damage-associated molecular pattern) release. The secretion of inflammatory cytokines and type I IFN recruits antigen presenting cells (APC) which present processed tumor antigens to T cells via MHC-I leading to a tumor antigen specific T cell response. The secretion of type I IFN additionally leads to the activation of T cells indicated by the expression of the early activation marker CD69. Tumor cell killing is likely to be mediated via MHC-I/TCR and Fas/FasL interaction, respectively. The therapy mediates a strong immunological memory indicating proper T cell priming and clonal expansion. α-PD-1 checkpoint inhibition improves the therapy´s efficacy by additional T cell activation.

8   Literature

Abdullahi, S., Jäkel, M., Behrend, S. J., Steiger, K., Topping, G., Krabbe, T., Colombo, A., Sandig, V., Schiergens, T. S., Thasler, W. E., Werner, J., Lichtenthaler, S. F., Schmid, R. M., Ebert, O. and Altomonte, M. (2018). A novel chimeric oncolytic virus vector for improved safety and efficacy in hepatocellular carcinoma. *Journal of Virology, 92*(23), e01386-01318.

Abou-Alfa, G. K., Schwartz, L., Ricci, S., Amadori, D., Santoro, A., Figer, A., De Greve, J., Douillard, J.-Y., Lathia, C., Schwartz, B., Taylor, I., Moscovici, M. and Saltz, L. B. (2006). Phase II study of sorafenib in patients with advanced hepatocellular carcinoma. *Journal of Clinical Oncology, 24*(26), 4293-4300.

Ahmad, S. and Hur, S. (2015). Helicases in antiviral immunity: dual properties as sensors and effectors. *Trends in Biochemical Sciences, 40*(10), 576-585.

Baird, J. R., Feng, Z., Xiao, H. D., Friedman, D., Cottam, B., Fox, B. A., Kramer, G., Leidner, R. S., Bell, R. B., Young, K. H., Crittenden, M. R. and Gough, M. J. (2017). STING expression and response to treatment with STING ligands in premalignant and malignant disease. *PLOS ONE, 12*(11), e0187532.

Beatty, G. L. and Gladney, W. L. (2015). Immune escape mechanisms as a guide for cancer immunotherapy. *Clinical Cancer Research, 21*(4), 687-692.

Bertuccio, P., Turati, F., Carioli, G., Rodriguez, T., La Vecchia, C., Malvezzi, M. and Negri, E. (2017). Global trends and predictions in hepatocellular carcinoma mortality. *Journal of Hepatology, 67*(2), 302-309.

Besch, R., Poeck, H., Hohenauer, T., Senft, D., Häcker, G., Berking, C., Hornung, V., Endres, S., Ruzicka, T., Rothenfusser, S. and Hartmann, G. (2009). Proapoptotic signaling induced by RIG-I and MDA-5 results in type I interferon–independent apoptosis in human melanoma cells. *The Journal of Clinical Investigation, 119*(8), 2399-2411.

Bibby, M. (2004). Orthotopic models of cancer for preclinical drug evaluation: advantages and disadvantages. *European Journal of Cancer, 40*(6), 852-857.

BioLegend. Mouse Alloantigens Retrieved July 27, 2018, from http://www.biolegend.com/media_assets/support_resource/BioLegend_Mouse_Alloan tigens.pdf

Bommareddy, P. K., Shettigar, M. and Kaufman, H. L. (2018). Integrating oncolytic viruses in combination cancer immunotherapy. *Nature Reviews Immunology, 18*(1), 498–513.

Buonaguro, L., Petrizzo, A., Tagliamonte, M., Tornesello, M. L. and Buonaguro, F. M. (2013). Challenges in cancer vaccine development for hepatocellular carcinoma. *Journal of Hepatology, 59*(4), 897-903.

Butterfield, L. H., Ribas, A., Meng, W. S., Dissette, V. B., Amarnani, S., Vu, H. T., Seja, E., Todd, K., Glaspy, J. A., McBride, W. H. and Economou, J. H. (2003). T-cell responses to HLA-A* 0201 immunodominant peptides derived from α-fetoprotein in patients with hepatocellular cancer. *Clinical Cancer Research, 9*(16), 5902-5908.

Chen, A., Zhang, Y., Meng, G., Jiang, D., Zhang, H., Zheng, M., Xia, M., Jiang, A., Wu, J., Beltinger, C. and Wei, J. (2017). Oncolytic measles virus enhances antitumour responses of adoptive CD8+ NKG2D+ cells in hepatocellular carcinoma treatment. *Scientific Reports, 7*(1), 5170.

Chen, J., Jin, R., Zhao, J., Liu, J., Ying, H., Yan, H., Zhou, S., Liang, Y., Huang, D., Liang, X., Yu, H., Lin, H. and Cai, X. (2015). Potential molecular, cellular and microenvironmental mechanism of sorafenib resistance in hepatocellular carcinoma. *Cancer Letters, 367*(1), 1-11.

Cheng, A.-L., Kang, Y.-K., Chen, Z., Tsao, C.-J., Qin, S., Kim, J. S., Luo, R., Feng, J., Ye, S., Yang, T.-S., Xu, J., Sun, Y., Liang, H., Liu, J., Wang, J., Tak, W. Y., Pan, H., Burock, K., Zou, J., Voliotis, D. and Guan, Z. (2009). Efficacy and safety of sorafenib in patients in the Asia-Pacific region with advanced hepatocellular carcinoma: a phase III randomised, double-blind, placebo-controlled trial. *The Lancet Oncology, 10*(1), 25-34.

ClinicalTrials.gov. (2018a) Retrieved May 27, 2018, from https://www.clinicaltrials.gov/ct2/results?term=pembrolizumab&cond=Hepatocellular+ Carcinoma&cntry=US

ClinicalTrials.gov. (2018b) Retrieved May 27, 2018, from https://www.clinicaltrials.gov/ct2/results?cond=Hepatocellular+Carcinoma&term=Nivol umab&cntry=US&state=&city=&dist=&Search=Search

ClinicalTrials.gov. (2018c). Phase I/II Trial of Intralesional Administration of RGT100 Retrieved July 26, 2018, from https://clinicaltrials.gov/ct2/show/NCT03065023

Deryugina, E. I. and Quigley, J. P. (2006). Matrix metalloproteinases and tumor metastasis. *Cancer and Metastasis Reviews, 25*(1), 9-34.

Diamond, M. S., Kinder, M., Matsushita, H., Mashayekhi, M., Dunn, G. P., Archambault, J. M., Lee, H., Arthur, C. D., White, J. M., Kalinke, U., Murphy, K. M. and Schreiber, R. D. (2011). Type I interferon is selectively required by dendritic cells for immune rejection of tumors. *Journal of Experimental Medicine, 208*(10), 1989-2003.

Duewell, P., Steger, A., Lohr, H., Bourhis, H., Hoelz, H., Kirchleitner, S., Stieg, M., Grassmann, S., Kobold, S., Siveke, J., Endres, S. and Schnurr, M. (2014). RIG-I-like helicases induce immunogenic cell death of pancreatic cancer cells and sensitize tumors toward killing by CD8+ T cells. *Cell Death and Differentiation, 21*(12), 1825.

Dusheiko, G. (1997). Side effects of α interferon in chronic hepatitis C. *Hepatology, 26*(S3), 112S-121S.

El-Khoueiry, A. B., Sangro, B., Yau, T., Crocenzi, T. S., Kudo, M., Hsu, C., Kim, T.-Y., Choo, S.-P., Trojan, J., Welling 3rd, T. H., Meyer, T., Kang, Y., Yeo, W., Chopra, A., Anderson, J., Dela Cruz, C., Lang, L., Neely, J., Tang, H., HB, D. and Melero, I. (2017). Nivolumab in patients with advanced hepatocellular carcinoma (CheckMate 040): an open-label, non-comparative, phase 1/2 dose escalation and expansion trial. *The Lancet, 389*(10088), 2492-2502.

Ellermeier, J., Wei, J., Duewell, P., Hoves, S., Stieg, M. R., Adunka, T., Noerenberg, D., Anders, H.-J., Mayr, D., Poeck, H., Hartmann, G., Endres, S. and Schnurr, M. (2013). Therapeutic efficacy of bifunctional siRNA combining TGF-β1 silencing with RIG-I activation in pancreatic cancer. *Cancer Research, 73*(6), 1709-1720.

European Medicines Agency. (2011). *Public summary of opinion on orphan designation - Sorafenib tosylate for the treatment of hepatocellular carcinoma.* EMA/COMP/95269/2006 Rev.3.

European Medicines Agency. (2017a). *Keytruda - EPAR summary for the public.* EMA/524789/2017.

European Medicines Agency. (2017b). *Opdivo (nivolumab) - EPAR summary for the public.* EMA/691693/2017.

Fatourou, E. M. and Koskinas, J. S. (2009). Adaptive immunity in hepatocellular carcinoma: prognostic and therapeutic implications. *Expert Review of Anticancer Therapy, 9*(10), 1499-1510.

Food and Drug Administration. (2013). *Nexavar (sorafenib) - highlights of prescribing information.* Reference ID: 3411803.

Food and Drug Administration. (2017a). *Keytruda® (pembrolizumab) - highlights of prescribing information.* Reference ID: 4156447

Food and Drug Administration. (2017b). *Opdivo (nivolumab) - highlights of prescribing information.* Reference ID: 4198384.

Fu, J., Kanne, D. B., Leong, M., Glickman, L. H., McWhirter, S. M., Lemmens, E., Mechette, K., Leong, J. J., Lauer, P., Liu, W., Sivick, K. E., Zeng, Q., Soares, K. C., Zheng, L., Portonoy, D. A., Woodward, J. J., Pardoll, D. M., Dubensky Jr., T. W. and Kim, Y. (2015). STING agonist formulated cancer vaccines can cure established tumors resistant to PD-1 blockade. *Science Translational Medicine, 7*(283), 283ra252-283ra252.

Fuertes, M. B., Kacha, A. K., Kline, J., Woo, S.-R., Kranz, D. M., Murphy, K. M. and Gajewski, T. F. (2011). Host type I IFN signals are required for antitumor CD8+ T cell responses through CD8α+ dendritic cells. *Journal of Experimental Medicine, 208*(10), 2005-2016.

Literature

Fuertes, M. B., Woo, S.-R., Burnett, B., Fu, Y.-X. and Gajewski, T. F. (2013). Type I interferon response and innate immune sensing of cancer. *Trends in Immunology, 34*(2), 67-73.

Funk, A. (2018). *RIG-I-like-Helikasen als Zielstrukturen für die Immuntherapie des hepatozellulären Karzinoms mittels bifunktioneller siRNA gegen Polo-like-Kinase 1.* Doctoral thesis, Ludwig-Maximilians-Universität München.

Gao, D.-Y., Lin, T.-T., Sung, Y.-C., Liu, Y. C., Chiang, W.-H., Chang, C.-C., Liu, J.-Y. and Chen, Y. (2015). CXCR4-targeted lipid-coated PLGA nanoparticles deliver sorafenib and overcome acquired drug resistance in liver cancer. *Biomaterials, 67*, 194-203.

Goodin, D., Neilley, L., Goodkin, D. and Hauser, S. (1995). Side-effect profile of interferon beta 1-B. *Journal of Neuroimmunology, 56*, 36.

Goubau, D., Schlee, M., Deddouche, S., Pruijssers, A. J., Zillinger, T., Goldeck, M., Schuberth, C., Van der Veen, A. G., Fujimura, T., Rehwinkel, J., Iskarpatyoti, J. A., Barchet, W., Ludwig, J., Dermody, T. S., Hartmann, G. and Reis e Sousa, C. (2014). Antiviral immunity via RIG-I-mediated recognition of RNA bearing 5′-diphosphates. *Nature, 514*(7522), 372.

Greten, T. F., Wang, X. W. and Korangy, F. (2015). Current concepts of immune based treatments for patients with HCC: from basic science to novel treatment approaches. *Gut, 64*(5), 2014-307990.

Hato, T., Goyal, L., Greten, T. F., Duda, D. G. and Zhu, A. X. (2014). Immune checkpoint blockade in hepatocellular carcinoma: current progress and future directions. *Hepatology, 60*(5), 1776-1782.

He, J.-D., Wang, Z., Li, S.-P., Xu, Y.-J., Yu, Y., Ding, Y.-J., Yu, W.-L., Zhang, R.-X., Zhang, H.-M. and Du, H.-Y. (2016). Vitexin suppresses autophagy to induce apoptosis in hepatocellular carcinoma via activation of the JNK signaling pathway. *Oncotarget, 7*(51), 84520.

He, L., Xiao, X., Yang, X., Zhang, Z., Wu, L. and Liu, Z. (2017). STING signaling in tumorigenesis and cancer therapy: A friend or foe? *Cancer Letters, 402*, 203-212.

Hölz, H. L. (2018). *Adjuvantes Interferon zur Optimierung RIG-I-basierter Immuntherapie des Pankreaskarzinoms.* Doctoral thesis, Ludwig-Maximilians-Universität München.

Hong, Y.-P., Li, Z.-D., Prasoon, P. and Zhang, Q. (2015). Immunotherapy for hepatocellular carcinoma: From basic research to clinical use. *World Journal of Hepatology, 7*(7), 980.

Hornung, V., Ellegast, J., Kim, S., Brzózka, K., Jung, A., Kato, H., Poeck, H., Akira, S., Conzelmann, K.-K., Schlee, M., Endres, S. and Hartmann, G. (2006). 5'-Triphosphate RNA is the ligand for RIG-I. *Science, 314*(5801), 994-997.

Hou, J., Zhou, Y., Zheng, Y., Fan, J., Zhou, W., Ng, I. O., Sun, H., Qin, L., Qiu, S., Lee, J. M., Lo, C.-M., Man, K., Yang, Y., Yang, Y., Yang, Y., Zhang, Q., Zhu, X., Li, N., Wang, Z., Ding, G., Zuang, S.-M., Zheng, L., Luo, X., Xie, Y., Liang, A., Wang, Z., Zhang, M., Xia, Q., Liang, T., Yu, Y. and Cao, X. (2014). Hepatic RIG-I predicts survival and interferon-α therapeutic response in hepatocellular carcinoma. *Cancer cell, 25*(1), 49-63.

Huang, Y., Cai, B., Xu, M., Qiu, Z., Tao, Y., Zhang, Y., Wang, J., Xu, Y., Zhou, Y., Yang, J., Han, X. and Gao, Q. (2012). Gene silencing of Toll-like receptor 2 inhibits proliferation of human liver cancer cells and secretion of inflammatory cytokines. *PLOS ONE, 7*(7), e38890.

Igney, F. H. and Krammer, P. H. (2002). Death and anti-death: tumour resistance to apoptosis. *Nature Reviews Cancer, 2*(4), 277.

Ikeguchi, M., Oi, K., Hirooka, Y. and Kaibara, N. (2004). CD8+ lymphocyte infiltration and apoptosis in hepatocellular carcinoma. *European Journal of Surgical Oncology, 30*(1), 53-57.

Iwasaki, A. and Medzhitov, R. (2010). Regulation of adaptive immunity by the innate immune system. *Science, 327*(5963), 291-295.

Kaczanowska, S., Joseph, A. M. and Davila, E. (2013). TLR agonists: our best frenemy in cancer immunotherapy. *Journal of Leukocyte Biology, 93*(6), 847-863.

Kanasty, R., Dorkin, J. R., Vegas, A. and Anderson, D. (2013). Delivery materials for siRNA therapeutics. *Nature Materials, 12*(11), 967.

Kane, R. C., Farrell, A. T., Madabushi, R., Booth, B., Chattopadhyay, S., Sridhara, R., Justice, R. and Pazdur, R. (2009). Sorafenib for the treatment of unresectable hepatocellular carcinoma. *The Oncologist, 14*(1), 95-100.

Kaneda, Y. (2013). The RIG-I/MAVS signaling pathway in cancer cell-selective apoptosis. *Oncoimmunology, 2*(4), e23566.

Kang, D., Gopalkrishnan, R. V., Lin, L., Randolph, A., Valerie, K., Pestka, S. and Fisher, P. B. (2004). Expression analysis and genomic characterization of human melanoma differentiation associated gene-5, mda-5: a novel type I interferon-responsive apoptosis-inducing gene. *Oncogene, 23*(9), 1789.

Kasai, K., Ushio, A., Kasai, Y., Sawara, K., Miyamoto, Y., Oikawa, K., Kuroda, H., Takikawa, Y. and Suzuki, K. (2012). Therapeutic efficacy of combination therapy with intra-arterial 5-fluorouracil and systemic pegylated interferon α-2b for advanced hepatocellular carcinoma with portal venous invasion. *Cancer, 118*(13), 3302-3310.

Khanna, C. and Hunter, K. (2005). Modeling metastasis in vivo. *Carcinogenesis, 26*(3), 513-523.

Krieg, A. M. (2008). Toll-like receptor 9 (TLR9) agonists in the treatment of cancer. *Oncogene, 27*(2), 161.

Kuang, P., Zhao, W., Su, W., Zhang, Z., Zhang, L., Liu, J., Ren, G., Yin, Z. and Wang, X. (2013). 18β-glycyrrhetinic acid inhibits hepatocellular carcinoma development by reversing hepatic stellate cell-mediated immunosuppression in mice. *International Journal of Cancer, 132*(8), 1831-1841.

Lazić, I. (2017). *Immuntherapie des hepatozellulären Karzinoms mit 5'-Triphosphat-modifizierter siRNA.* Doctoral thesis, Ludwig-Maximilians-Universität München.

Lee, D., Chung, Y. H., Kim, J. A., Park, W. H., Jin, Y. J., Shim, J. H., Ryu, S. H., Jang, M. K., Yu, E. and Lee, Y. J. (2013). Safety and efficacy of adjuvant pegylated interferon therapy for metastatic tumor antigen 1-positive hepatocellular carcinoma. *Cancer, 119*(12), 2239-2246.

Leenders, M. W., Nijkamp, M. W. and Rinkes, I. H. B. (2008). Mouse models in liver cancer research: a review of current literature. *World Journal of Gastroenterology, 14*(45), 6915.

Leitlinienprogramm Onkologie. (2013). Diagnostik und Therapie des hepatozellulären Karzinoms (Deutsche Krebsgesellschaft, Deutsche Krebshilfe, AWMF). *Zeitschrift für Gastroenterologie, 51*(11), 1269-1326.

Li, D., Li, N., Zhang, Y., Fu, H., Torres, M. B., Wang, Q., Greten, T. F. and Ho, M. (2018). Abstract 2549: Development of CAR T-cell therapy targeting glypican-3 in liver cancer. *Cancer Research, 78*(13), 2549.

Li, L. and Wang, H. (2016). Heterogeneity of liver cancer and personalized therapy. *Cancer Letters, 379*(2), 191-197.

Li, M., Lu, C., Cheng, J., Zhang, J., Cao, C., Xu, J., Xu, J., Pan, H., Zhong, B., Tucker, S. and Wang, D. (2009). Combination therapy with transarterial chemoembolization and interferon-α compared with transarterial chemoembolization alone for hepatitis B virus related unresectable hepatocellular carcinoma. *Journal of Gastroenterology and Hepatology, 24*(8), 1437-1444.

Liu, Z., Dou, C., Jia, Y., Li, Q., Zheng, X., Yao, Y., Liu, Q. and Song, T. (2015). RIG-I suppresses the migration and invasion of hepatocellular carcinoma cells by regulating MMP9. *International Journal of Oncology, 46*(4), 1710-1720.

Llovet, J. M., Ricci, S., Mazzaferro, V., Hilgard, P., Gane, E., Blanc, J.-F., de Oliveira, A. C., Santoro, A., Raoul, J.-L., Forner, A., Schwartz, M., Porta, C., Zeuzem, S., Bolondi, L., Greten, T. F., Galle, P. R., Seitz, J.-F., Borbath, I., Häussinger, D., Giannaris, T., Shan, M., Moscovici, M., Voliotis, D. and Bruix, J. (2008). Sorafenib in advanced hepatocellular carcinoma. *New england Journal of Medicine, 359*(4), 378-390.

Loo, Y.-M. and Gale Jr, M. (2011). Immune signaling by RIG-I-like receptors. *Immunity, 34*(5), 680-692.

Luo, D., Ding, S. C., Vela, A., Kohlway, A., Lindenbach, B. D. and Pyle, A. M. (2011). Structural insights into RNA recognition by RIG-I. *Cell, 147*(2), 409-422.

Lygidakis, N. J., Kosmidis, P., Ziras, N., Parissis, J. and Kyparidou, E. (1995). Combined transarterial targeting locoregional immunotherapy-chemotherapy for patients with unresectable hepatocellular carcinoma: a new alternative for an old problem. *Journal of Interferon and Cytokine Research, 15*(5), 467-472.

Ma, S., Cheng, Q., Cai, Y., Gong, H., Wu, Y., Yu, X., Shi, L., Wu, D., Dong, C. and Liu, H. (2014). IL-17A produced by γδ T cells promotes tumor growth in hepatocellular carcinoma. *Cancer Research, 74*(7), 1969-1982.

Makarova-Rusher, O. V., Medina-Echeverz, J., Duffy, A. G. and Greten, T. F. (2015). The yin and yang of evasion and immune activation in HCC. *Journal of Hepatology, 62*(6), 1420-1429.

Matsushima-Miyagi, T., Hatano, K., Nomura, M., Li-Wen, L., Nishikawa, T., Saga, K., Shimbo, T. and Kaneda, Y. (2012). TRAIL and/or Noxa are selectively up-regulated in prostate cancer cells downstream of the RIG-I/MAVS signaling pathway by non-replicating Sendai virus particles. *Clinical Cancer Research, 18*(22), 6271–6283.

Maus, M. V., Grupp, S. A., Porter, D. L. and June, C. H. (2014). Antibody modified T cells: CARs take the front seat for hematologic malignancies. *Blood, 123*(17), 2625-2635.

Meng, G., Xia, M., Xu, C., Yuan, D., Schnurr, M. and Wei, J. (2014). Multifunctional antitumor molecule 5′-triphosphate siRNA combining glutaminase silencing and RIG-I activation. *International Journal of Cancer, 134*(8), 1958-1971.

Merle, P., Si Ahmed, S., Habersetzer, F., Abergel, A., Taieb, J., Bonyhay, L., Costantini, D., Dufour-Lamartinie, J. and Trepo, C. (2006). Phase 1 study of intra-arterial hepatic (IAH) delivery of doxorubicin-transdrug (DT) for patients with advanced hepatocellular carcinoma (HCC). *Journal of Clinical Oncology, 24*, 14094-14094.

O'connell, J., O'sullivan, G. C., Collins, J. K. and Shanahan, F. (1996). The Fas counterattack: Fas-mediated T cell killing by colon cancer cells expressing Fas ligand. *Journal of Experimental Medicine, 184*(3), 1075-1082.

Obi, S., Yoshida, H., Toune, R., Unuma, T., Kanda, M., Sato, S., Tateishi, R., Teratani, T., Shiina, S. and Omata, M. (2006). Combination therapy of intraarterial 5-fluorouracil and systemic interferon-alpha for advanced hepatocellular carcinoma with portal venous invasion. *Cancer, 106*(9), 1990-1997.

PerkinElmer Inc. (2013). Application Note - Pre-clinical *in vivo* imaging, Bioimaging of Gene Delivery with *In Vivo*-jetPEI®.

Petrocca, F. and Lieberman, J. (2008). RIG-ing an antitumor response. *Nature Medicine, 14*(11), 1152.

Picaud, S., Bardot, B., De Maeyer, E. and Seif, I. (2002). Enhanced tumor development in mice lacking a functional type I interferon receptor. *Journal of Interferon and Cytokine Research, 22*(4), 457-462.

Pinter, M., Sieghart, W., Graziadei, I., Vogel, W., Maieron, A., Königsberg, R., Weissmann, A., Kornek, G., Plank, C. and Peck-Radosavljevic, M. (2009). Sorafenib in unresectable hepatocellular carcinoma from mild to advanced stage liver cirrhosis. *The Oncologist, 14*(1), 70-76.

Poeck, H., Besch, R., Maihoefer, C., Renn, M., Tormo, D., Morskaya, S. S., Kirschnek, S., Gaffal, E., Landsberg, J., Hellmuth, J., Schmidt, A., Anz, D., Bscheider, M., Schwerd, T., Berking, C., Bourquin, C., Kalinke, U., Kremmer, E., Kato, H., Akira, S., Meyer, R., Häcker, G., Neuenhahn, M., Busch, D., Ruland, J., Rotehnfusser, S., Prinz, M., Hornung, V., Endres, S., Türing, T. and Hartmann, G. (2008). 5′-Triphosphate-siRNA: turning gene silencing and Rig-I activation against melanoma. *Nature Medicine, 14*(11), 1256.

Pol, J., Kroemer, G. and Galluzzi, L. (2016). First oncolytic virus approved for melanoma immunotherapy. *Oncoimmunology, 5*(1), e1115641.

Prieto, J., Melero, I. and Sangro, B. (2015). Immunological landscape and immunotherapy of hepatocellular carcinoma. *Nature Reviews Gastroenterology and Hepatology, 12*(12), 681.

Rao, Q., You, A., Guo, Z., Zuo, B., Gao, X., Zhang, T., Du, Z., Wu, C. and Yin, H. (2016). Intrahepatic tissue implantation represents a favorable approach for establishing orthotopic transplantation hepatocellular carcinoma mouse models. *PLOS ONE, 11*(1), e0148263.

Reddy, L. H. and Couvreur, P. (2011). Nanotechnology for therapy and imaging of liver diseases. *Journal of Hepatology, 55*(6), 1461-1466.

Sakon, M., Nagano, H., Dono, K., Nakamori, S., Umeshita, K., Yamada, A., Kawata, S., Imai, Y., Iijima, S. and Monden, M. (2002). Combined intraarterial 5-fluorouracil and subcutaneous interferon-α therapy for advanced hepatocellular carcinoma with tumor thrombi in the major portal branches. *Cancer, 94*(2), 435-442.

Sangro, B., Mazzolini, G., Ruiz, J., Herraiz, M., Quiroga, J., Herrero, I., Benito, A., Larrache, J., Pueyo, J., Subtil, J. C., Olagüe, C., Sola, J., Sádaba, B., Lacasa, C., Melero, I., Qian, C. and Prieto, J. (2004). Phase I trial of intratumoral injection of an adenovirus encoding interleukin-12 for advanced digestive tumors. *Journal of Clinical Oncology, 22*(8), 1389-1397.

Sanmamed, M., Chester, C., Melero, I. and Kohrt, H. (2016). Defining the optimal murine models to investigate immune checkpoint blockers and their combination with other immunotherapies. *Annals of Oncology, 27*(7), 1190-1198.

Sanyal, A. J., Yoon, S. K. and Lencioni, R. (2010). The etiology of hepatocellular carcinoma and consequences for treatment. *The Oncologist, 15*(4), 14-22.

Schmidt, A., Schwerd, T., Hamm, W., Hellmuth, J. C., Cui, S., Wenzel, M., Hoffmann, F. S., Michallet, M.-C., Besch, R., Hopfner, K.-P., Endres, S. and Rothenfusser, S. (2009). 5′-triphosphate RNA requires base-paired structures to activate antiviral signaling via RIG-I. *Proceedings of the National Academy of Sciences, 106*(29), 12067-12072.

Sharpe, A. H. (2017). Introduction to checkpoint inhibitors and cancer immunotherapy. *Immunological Reviews, 276*(1), 5-8.

Siegel, R. L., Miller, K. D. and Jemal, A. (2015). Cancer statistics, 2015. *CA: A Cancer Journal for Clinicians, 65*(1), 5-29.

Slotta, J. E., Kollmar, O., Ellenrieder, V., Ghadimi, B. M. and Homayounfar, K. (2015). Hepatocellular carcinoma: Surgeon's view on latest findings and future perspectives. *World Journal of Hepatology, 7*(9), 1168.

Tada, F., Abe, M., Hirooka, M., Ikeda, Y., Hiasa, Y., Lee, Y., Jung, N.-C., Lee, W.-B., Lee, H.-S., Bae, Y.-S. and Onji, M. (2012). Phase I/II study of immunotherapy using tumor antigen-pulsed dendritic cells in patients with hepatocellular carcinoma. *International Journal of Oncology, 41*(5), 1601-1609.

Takeda, K. and Akira, S. (2004). *TLR signaling pathways.* Paper presented at the Seminars in Immunology.

Takeuchi, O. and Akira, S. (2008). MDA5/RIG-I and virus recognition. *Current Opinion in Immunology, 20*(1), 17-22.

Truong, P., Rahal, A. and Kallail, K. J. (2016). Metastatic hepatocellular carcinoma responsive to pembrolizumab. *Cureus, 8*(6), e631.

Venook, A. P., Papandreou, C., Furuse, J. and de Guevara, L. L. (2010). The incidence and epidemiology of hepatocellular carcinoma: a global and regional perspective. *The Oncologist, 15*(4), 5-13.

Vesely, M. D., Kershaw, M. H., Schreiber, R. D. and Smyth, M. J. (2011). Natural innate and adaptive immunity to cancer. *Annual Review of Immunology, 29*, 235-271.

Wong, M. C., Jiang, J. Y., Goggins, W. B., Liang, M., Fang, Y., Fung, F. D., Leung, C., Wang, H. H., Wong, G. L. and Wong, V. W. (2017). International incidence and mortality trends of liver cancer: a global profile. *Scientific Reports, 7*, 45846.

Yau, T., Chan, P., Ng, K. K., Chok, S. H., Cheung, T. T., Fan, S. T. and Poon, R. T. (2009). Phase 2 open-label study of single-agent sorafenib in treating advanced hepatocellular carcinoma in a hepatitis B–endemic Asian population. *Cancer, 115*(2), 428-436.

Zhang, B. and Finn, R. S. (2016). Personalized clinical trials in hepatocellular carcinoma based on biomarker selection. *Liver Cancer, 5*(3), 221-232.

Zhang, H., Li, K., Lin, Y., Xing, F., Xiao, X., Cai, J., Zhu, W., Liang, J., Tan, Y., Fu, L., Wang, F., Yin, W., Lu, B., Qiu, P., Su, X., Gong, S., Bai, X., Hiu, J. and Yan, G. (2017). Targeting VCP enhances anticancer activity of oncolytic virus M1 in hepatocellular carcinoma. *Science Translational Medicine, 9*(404), 7996.

Zhang, W., Sun, H. C., Wang, W. Q., Zhang, Q. B., Zhuang, P. Y., Xiong, Y. Q., Zhu, X. D., Xu, H. X., Kong, L. Q., Wu, W. Z., Wang, L., Song, T.-Q., Li, Q. and Tang, Z.-Y. (2012). Sorafenib down-regulates expression of HTATIP2 to promote invasiveness and metastasis of orthotopic hepatocellular carcinoma tumors in mice. *Gastroenterology, 143*(6), 1641-1649. e1645.

Zou, H., Wang, W.-K., Liu, Y.-L., Braddock, M., Zheng, M.-H. and Huang, D.-S. (2016). Toll-like receptors in hepatocellular carcinoma: potential novel targets for pharmacological intervention. *Expert Opinion on Therapeutic Targets, 20*(9), 1127-1135.

9 Appendix

9.1 Abbreviations

actb	Gene that encodes β-actin
AKT	Protein kinase B
ANOVA	Analysis of variance
ASGP-R	Asialoglycoprotein receptor
BSC	Best supportive care
BSA	Bovine serum albumin
CAR	Chimeric antigen receptor
CARD	Caspase recruitment domain
CD	Cluster of differentiation
cDNA	Copy deoxyribonucleic acid
cGas	Cyclic GMP-AMP synthase
CIK	Cytokine-induced killer cells
c-Met	Cellular mesenchymal–epithelial transition
CT	Computed tomography
CTD	C-terminal regulatory domain
CXCL10	C-X-C motif chemokine 10 (also known as IP-10)
DAMP	Damage-associated molecular pattern
DC	Dendritic cell
ddx58	Gene that encodes RIG-I
DMEM	Dulbecco's modified Eagle's medium
DMSO	Dimethylsulfoxide
EDTA	Ethylenediamine tetraacetic acid
ELISA	Enzym-linked immunosorbent assay
EMA	European Medicine Agency
ERK	Extracellular signal-regulated kinase
FACS	Fluorescence activated cell sorter
Fas	Fas cell surface death receptor (also known as CD95)
FasL	Fas ligand
FBS	Fetal bovine serum
FDA	Food and Drug Administration
FoxP3	Forkhead box P3
GOT	Glutamic oxaloacetic transaminase
GPC3	Glypican 3

Appendix

GPT	Glutamaic pyruvic transaminase
HBV	Hepatitis B virus
HCC	Hepatocellular carcinoma
HCV	Hepatitis C virus
HLA	Human leukocyte antigen
HRP	Horse radish peroxidase
HSC	Hepatic stellate cell
i.p.	Intraperitoneal
i.v.	Intravenous
IFNAR	Interferon-α receptor
ifnb1	Gene that encodes IFN-β
IFN-α	Interferon α
IFN-β	Interferon β
IgG	Immunoglobulin G
IL	Interleukin
IP-10	Interferon gamma-induced protein 10 (also known as CXCL10)
IRF	IFN regulatory factor
ISG	Interferon stimulated gene
JNK	Jun N-terminal kinase
KO	Knock-out
LGP2	Laboratory of Genetics and Physiology 2
LSEC	Liver sinusoidal endothelial cell
mAb	Monoclonal antibody
MAPK	Mitogen-activated protein kinase
MAVS	Mitochondrial antiviral-signaling protein
MDA5	Melanoma differentiation-associated gene 5
MDSC	Myeloid-derived suppressor cell
MFI	Median fluorescence intensity
MHC	Major histocompatibility complex
MMP	Matrix metalloproteinase
mRNA	Messenger RNA
NAFLD	Non-alcoholic fatty liver disease
NASH	Non-alcoholic steatohepatitis
NF-κB	Nuclear factor kappa-light-chain-enhancer of activated B-cells
NK cell	Natural killer cell
Nod	Non-obese diabetic

Appendix

NP-40	Nonidet P-40
NSG mouse	Nod-*scid* mouse
OH-RNA	Unspecific control RNA without 5'ppp-modification
OS	Overall survival
OV	Onkolytic virus
PAMP	Pathogen-associated molecular pattern
PB	Pacific blue
PBS	Phosphate-buffered saline
PD-1	Programmed cell death protein 1
PD-L1	Programmed cell death ligand 1
PE	Phycoerythin
PEI	Percutaneous ethanol injection
PerCP	Peridinin chlorophyll
PFA	Paraformaldehyde
PFA	Paraformaldehyde
PFS	Progression free survival
PFS	Progression free survival
PI	Propidium iodide
pIRF-3	Phosphorylated IRF-3
ppp-RNA	5´-triphosphate-RNA
PRR	Pattern recognition receptors
qRT-PCR	Quantitative real time PCR
RAS	Rat sarcoma
RFA	Radio frequency ablation
RIG-I	Retinoic acid-inducible gene I
RIPA	Radioimmunoprecipitation assay
RISC	RNA-induced silencing complex
RLH	RIG-I-like helicases
RNAi	RNA interference
RPMI	Roswell Park Memorial Institue
s.c.	Subcutaneous
Scid	Severe combined immunodeficiency
SDS	Sodium dodecyl sulfate
SEM	Standard error of the mean
siRNA	Short interfering RNA
SMAD	Contraction of Sma and Mad

Appendix

STING	Stimulator of interferon genes
TAA	Tumor-associated antigens
TACE	Transarterial chemoembolization
TBS	Tris-buffered saline
TBS-T	Tris-buffered saline with Tween 20
T_{eff}	Effector T cells
TGF-β	Transforming growth factor β
TIL	Tumor infiltrating lymphocytes
TMA	Tissue micro array
T_{reg}	Regulatory T cell
VEGFR	Vascular endothelial growth factor receptor
Wt	Wild-type

9.2   List of figures

9.3 List of tables

9.4 Publication

9.4.1 Original publication

Ardelt M., Fröhlich T., Martini E., Müller M., Kanitz V., Atzberger C., Cantonati P., Meßner M., Posselt L., Lehr T., Wojtyniak J., Ulrich M., Arnold G., König L., Parazzoli D., Zahler S., Rothenfußer S., Mayr D., Gerbes A., Scita G., Vollmar A., Pachmayr J. (2018). Inhibition of cyclin-dependent kinase 5 – a novel strategy to improve sorafenib response in HCC therapy. *Hepatology.* 2018 Jul 23. doi: 10.1002/hep.30190 [Epub ahead of print].

9.4.2 Conference posters

Posselt L., Lazic I., Boehmer D., Funk A, Kirchleitner S., Hoffmann S., Adunka T., Endres S., Düwell P., Rothenfusser S., Schnurr M. Targeting RIG-I with 5'ppp-modified RNA for immunotherapy of hepatocellular carcinoma (HCC). ImmunoFest Munich 2014, September 2014.

Posselt L., Lazic I., Boehmer D., Funk A, Kirchleitner S., Hoffmann S., Adunka T., Endres S., Düwell P., Rothenfusser S., Schnurr M. Targeting RIG-I with 5'ppp-modified RNA for immunotherapy of hepatocellular carcinoma (HCC). 42. Jahrestagung der Gesellschaft für Gastroenterologie in Bayern, October 2014.

Posselt L., Lazic I., Boehmer D., Hoffmann S., Endres S., Duewell P., Rothenfusser S., Schnurr M. Therapy of hepatocellular carcinoma (HCC) with immunostimulatory RNA activating RIG-I. The Immunotherapy of Cancer Conference 2015, March 2015.

Posselt L., Lazic I., Boehmer D., Hoffmann s., Duewell P., Koenig L., Endres S., Rothenfusser S., Schnurr M. RIG-I based immunotherapy of hepatocellular carcinoma (HCC). CIMT Annual Meeting 2015, May 2015.

Posselt L., Lazic I., Boehmer D., Hoffmann S., Duewell P., Endres S., Rothenfusser S., Schnurr M., Koenig L. Therapy of Hepatocellular carcinoma (HCC) targeting RIG-I with 5´ppp-RNA. TOLL 2015 Meeting, September/October 2015.

Posselt L.[*], Orth M.[*], Belka C, Kirchleitner S., Schuster J., Endres S., Duewell P., Lauber K. and Schnurr M. Targeting DNA damage response genes to improve radiotherapy of pancreatic cancer; CIMT Annual Meeting 2016, May 2016.

[*] *Equal contribution*

9.5   Acknowledgement